
Disclaimer

This manuscript has been published in NATURE COMMUNICATIONS EARTH & ENVIRONMENT. The final version of this manuscript is available as: **Rovere, A., Pappalardo, M., Richiano, S. et al. Higher than present global mean sea level recorded by an Early Pliocene intertidal unit in Patagonia (Argentina). Commun Earth Environ 1, 68 (2020). <https://doi.org/10.1038/s43247-020-00067-6>**

Please feel free to contact any of the authors with feedback and suggestions for improvements.

Document history

Date	Action
1/Jul/2020	MS sent to co-authors for final draft acceptance
3/Jul/2020	IGSN for samples requested Spreadsheet and scripts submitted to Zenodo MS Submitted to EarthArXiv
8/Jul/2020	Preprint DOI Received MS Submitted to Nature Geoscience
14/Jul/2020	IGSN received and inserted for all samples Small style adjustments to tables
21/Jul/2020	Received initial decision from Nature Geoscience Transferred to Nature Communications
29/Jul/2020	Sent to reviewers by Nature Communications
3/Sept/2020	Reviews received, pending transfer to other journal
15/Oct/2020	Scripts and data updated in Zenodo, last check by first author
21/Oct/2020	Reviews completed, paper transferred to Communications Earth and Environment with answer to reviewers comments
3/Nov/2020	Revised version uploaded to EarthArxiv Title has been updated as per journal editorial team request
23/Dec/2020	Published in Nature Comms Earth and Environment

HIGHER THAN PRESENT GLOBAL MEAN SEA LEVEL RECORDED BY AN EARLY PLIOCENE INTERTIDAL UNIT IN PATAGONIA (ARGENTINA).

PREPRINT, COMPILED DECEMBER 26, 2020

Alessio Rovere¹, Marta Pappalardo², Sebastian Richiano³, Marina Aguirre^{4,5}, Michael R. Sandstrom⁶, Paul J. Hearty⁷, Jacqueline Austermann⁶, Ignacio Castellanos⁵, and Maureen E. Raymo⁶

¹MARUM - Center for Marine Environmental Sciences, University of Bremen. Leobener Str. 8., D-28359, Bremen, Germany

²Department of Earth Sciences, Università degli studi di Pisa. Via S. Maria 53, 56126, Pisa Italy

³Instituto Patagónico de Geología y Paleontología, CONICET. Bv. Almirante Brown 2915, Puerto Madryn (9120), Chubut, Argentina

⁴CONICET, CCT-La Plata and Universidad Nacional de La Plata. Calle 8 n.1467, B1904CMC, La Plata, Buenos Aires, Argentina

⁵Facultad de Ciencias Naturales y Museo, Universidad Nacional de La Plata. Calle 64 n.3, 1900 La Plata, Buenos Aires, Argentina

⁶Lamont Doherty Earth Observatory, Columbia University. 61 Rte 9W, Palisades, NY 10964, United States

⁷Department of Geological Sciences, Jackson School of Geosciences, The University of Texas at Austin. 2275 Speedway Stop C9000, Austin, Texas, United States

ABSTRACT

NOTE FOR THE READER: this is a preprint of a paper published in Nature Communications Earth & Environment. The final, peer-reviewed and proof-read paper is available at this link: <https://doi.org/10.1038/s43247-020-00067-6>.

Reconstructions of global mean sea level from earlier warm periods in Earth's history can help constrain future projections of sea level rise. Here we report on the sedimentology and age of a geological unit in central Patagonia, Argentina, that we dated to the Early Pliocene (4.69-5.23 Ma, 2σ) with strontium isotope stratigraphy. The unit was interpreted as representative of an intertidal environment, and its elevation was measured with differential GPS at ca. 36 m above present-day sea level. Considering modern tidal ranges, it was possible to constrain paleo relative sea level within $\pm 2.7\text{m}$ (1σ). We use glacial isostatic adjustment models and estimates of vertical land movement to calculate that, when the Camarones intertidal sequence was deposited, global mean sea level was $28.4 \pm 11.7\text{m}$ (1σ) above present. This estimate matches those derived from analogous Early Pliocene sea level proxies in the Mediterranean Sea and South Africa. Evidence from these three locations indicates that Early Pliocene sea level may have exceeded 20m above its present level. Such high global mean sea level values imply an ice-free Greenland, a significant melting of West Antarctica, and a contribution of marine-based sectors of East Antarctica to global mean sea level.

Keywords Early Pliocene · Sea level · Stratigraphy

1 INTRODUCTION

2 The survey, interpretation and dating of paleo relative sea level
3 (RSL) indicators (such as fossil coral reefs or relic beach de-
4 posits¹) is paramount to constraining the maximum elevation
5 reached by global mean sea level during periods of the Earth's
6 history warmer than the pre-industrial. The elevation of paleo
7 RSL indicators is the only direct proxy available to estimate
8 global mean sea level in Earth's past. Once measured, observed
9 paleo RSL indicators must be corrected for processes causing
10 "*Departures from Eustasy*"² (such as tectonics, mantle dynamic
11 topography, DT, and glacial isostatic adjustment, GIA^{3,4}) to
12 obtain paleo global mean sea level (GMSL) estimates. These
13 are in turn important to informing models of ice sheet melting
14 under future warmer climates⁵.

15 A recent global database⁶ shows that about 5000 RSL indica-
16 tors were preserved since the Last Glacial Maximum (30 ka).
17 Well-preserved and dated RSL indicators are relatively rare for
18 older time periods: another compilation of Pleistocene RSL in-
19 dicators⁷ reports more than 1000 Last Interglacial (MIS 5e, 125
20 ka) and only around 20 MIS 11 (400 ka) RSL indicators. Only a
21 handful of sites exist that document sea level highstands beyond
22 one million years ago^{2;8;9;10;11}. In general, robust RSL indica-

tors predating 400 ka are rare to find because they are poorly
preserved and are most often difficult to date with precision.
Additionally, relating them to GMSL is difficult since they are
likely affected by significant post-depositional movements. This
limits our ability to gauge the sensitivity of ice caps to warmer
climate conditions, such as those that characterized Earth in the
Pliocene.

Some of the oldest, precisely dated and measured RSL indicators
were recently reported on the island of Mallorca (Balearic Is-
lands, Spain), in a coastal cave called "*Coves d'Artá*". Here, six
phreatic overgrowths on speleothems mark the paleo water/air
interface within the cave⁹, and are therefore closely related to
paleo RSL. The highest and oldest of these formations was mea-
sured at $31.8 \pm 0.25\text{m}$ above mean sea level, and yielded a U-Pb
age of $4.29 \pm 0.39\text{Ma}$ (2σ)⁹. Taking into account GIA and
possible long-term deformation due to tectonics or dynamic to-
pography, it was estimated that global mean sea level at the time
of deposition of this RSL indicator was 25.1m above present,
bounded by uncertainties represented by 16th-84th percentiles
of 10.6-28.3m⁹. For the same time period, a second study¹⁰
reported a site in the Republic of South Africa (Northern Cape
Province, site Cliff Point-ZCP Section2). Here, oyster shells liv-

23
24
25
26
27
28
29
30
31
32
33
34
35
36
37
38
39
40
41
42
43
44

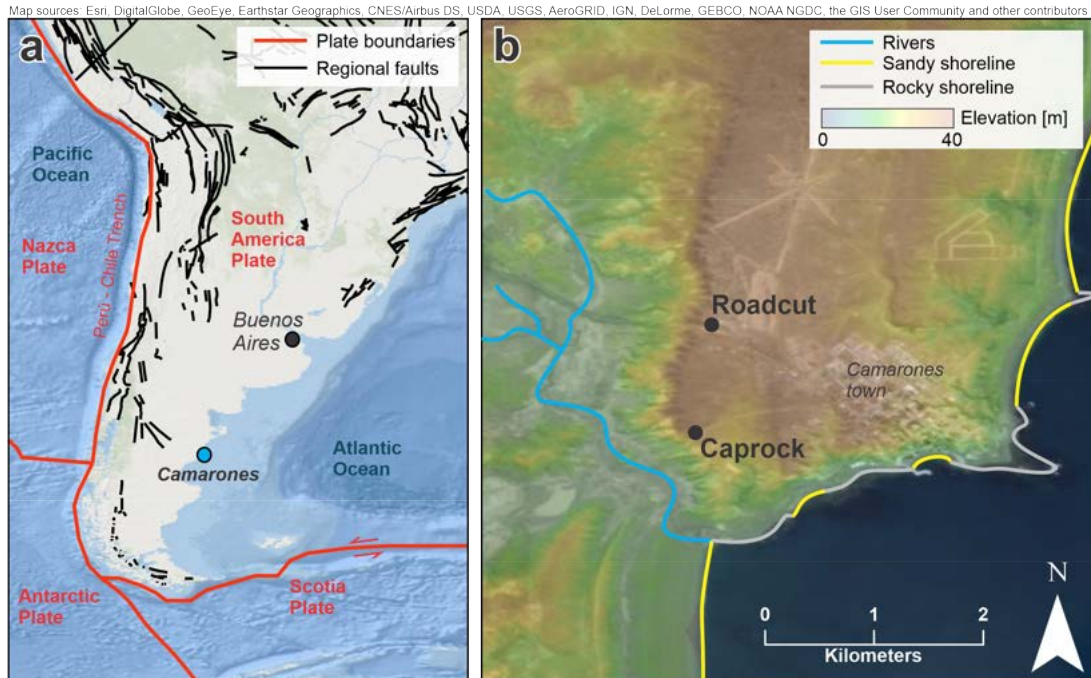


Figure 1: General and specific location of the study area. **a)** Location of the study area and main geological structures in the Southern part of South America. **b)** Topography of the Camarones town area, with location of the two outcrops (*Roadcut* and *Caprock*) presented in this study. Map sources: Esri, DigitalGlobe, GeoEye, Earthstar Geographics, CNES/Airbus DS, USDA, USGS, AeroGRID, IGN, DeLorme, GEBCO, NOAA NGDC, SRTM, the GIS User Community and other contributors. Elevation data in B are from the Shuttle Radar Topography Mission¹².

45 ing in a paleo subtidal to intertidal environment constrain paleo
 46 RSL at 35.1 ± 2.2 m (1σ). The oysters were dated to 4.28-4.87
 47 Ma (2σ range) with strontium isotope stratigraphy (SIS). While
 48 paleo global mean sea level estimates were not calculated at
 49 this site, based on the Mallorca benchmark the authors argue
 50 that this location was affected by relatively minor vertical land
 51 movements (possibly uplift) since 5 Ma.

52 While indirect paleo sea level estimates spanning the last 5.3 Ma
 53 are available from oxygen isotopes^{13;14;15}, the two studies cited
 54 above are arguably the only ones reporting relatively precise and
 55 well-dated direct sea-level observations for the Early Pliocene,
 56 that is regarded as a past analogue for future warmer climate¹⁶.
 57 At this time, CO₂ was between pre-industrial and modern levels,
 58 with possibly higher peaks to 450 ppm^{17;16}. During Early
 59 Pliocene interglacials, average global temperatures were 2-3°C
 60 higher than pre-industrial values^{18;16}. Pliocene climate was
 61 modulated by a ca. 40 kyr periodicity in glacial/interglacial
 62 cycles with highstands and lowstands that were characterized by
 63 sea-level oscillations as high as 13 ± 5 m¹⁹. Ice models suggest
 64 that, during the warmest Pliocene interglacials, Greenland was
 65 ice-free²⁰. Similarly, they suggest that the West Antarctic Ice
 66 sheet was likely subject to periodic collapses²¹, and might have
 67 contributed as much as 7 m²² to GMSL. Ice models and field-
 68 based evidence²³ suggest that also the East Antarctic Ice Sheet
 69 might have been smaller than today, contributing another 3 m²²
 70 to 13-16 m²⁴ to GMSL.

71 In this study, we report a foreshore (intertidal) sequence located
 72 in the town of Camarones, along the coast of central Patagonia,
 73 Argentina (Figure 1). Combining field data, SIS ages, GIA and

DT models we conclude that this deposit formed 4.69-5.23 Ma
 ago (2σ range) when sea level was 28.4 ± 11.7 (1σ) higher
 than today. This estimate is broadly consistent with those derived
 from the Republic of South Africa and Spain. Together, these three
 studies present a coherent picture of global mean sea level during
 the Early Pliocene, that likely exceeded 20m above modern sea
 level.

STUDY AREA: CAMARONES, CENTRAL PATAGONIA, ARGENTINA

The Patagonia geographic region includes territories belonging to the states of Argentina and Chile. Geologically, Patagonia represents the southernmost tip of the South American plate (Figure 1a). Along the Pacific coasts of Patagonia, the Nazca and the Antarctic plates are subducting below the Andes. Towards the south, the Scotia plate moves eastward and outlines Tierra del Fuego, at South America's southern tip²⁵. To the East, the Patagonian Atlantic coast is a passive margin, tectonically characterized as an extensional stress field and bordered by a wide continental shelf. The central and eastern parts of this landmass are represented by the Andean foreland, formed by a Palaeozoic-Mesozoic metamorphic basement overlapped by Tertiary continental and marine sedimentary rocks, dating back to the Paleocene. These are covered by Eocene-Oligocene pyroclastic rocks and Middle Miocene fluvial sediments. Marine sedimentary rocks corresponding to Tertiary transgressions are located east of the Andean foreland²⁶. In the Middle Miocene, the Chile Triple Junction migrated northward, leading to the opening of an asthenospheric window below southern Patagonia



Figure 2: The *Roadcut* outcrop at Camarones. The inset shows a detail of Unit **Cp**, a shelly-rich layer interpreted as representative of a foreshore (intertidal) environment dating to the Early Pliocene. Each unit is described in details in the Supplementary Note 2, including descriptions of the *Caprock* outcrop.

102 nia²⁷. This caused a switch from subsidence to uplift, and the
103 Patagonia region underwent a moderate but continuous uplift.²⁸

104 Along the coastlines of Central Patagonia, several levels of paleo
105 shorelines above modern sea level were noted by Charles Darwin
106 in his Beagle voyage²⁹, and were the subject of more than 150
107 years of research (See Supplementary Note 1 and Supplementary
108 Table 1). Studies of Pleistocene coastal sequences in Central
109 Patagonia include outcrops of Holocene^{30;31}, Pleistocene^{32;33;34}
110 and Pliocene-to-Miocene^{35;36} age. Among the latter, Del Río et
111 al. (2013)³⁶ dated Early Pliocene mollusks from marine deposits
112 few hundreds of kilometers south of the study area described in
113 this study.

114 The town of Camarones lies at the northern tip of the San Jorge
115 Gulf, approximately 1300 km south of Buenos Aires. Within a
116 few kilometers of Camarones, several paleo-sea level indicators
117 have been preserved, from the Holocene³⁷ to the Pleistocene³².
118 Already in the late 1940s, the Italian geologist Feruglio³⁸ iden-
119 tified an elevated marine terrace along a roadcut carved on the
120 main road leading into the town of Camarones that he tenta-
121 tively attributed to the Pliocene. He called this terrace, the
122 Camarones High Terrace (originally, in Spanish, *Teraza Alta de*
123 *Camarones*³⁸). A recent study³² confirmed the elevation of the
124 Camarones High Terrace at ca. 40m above sea level, at the lower
125 bound of the "beach barriers and terrace deposits between 40
126 and 110m elevation" reported by the 1:250.000 geological chart
127 of Camarones³⁹.

RESULTS: THE PLIOCENE SEA LEVEL RECORD AT CAMARONES AND GMSL ESTIMATES

128
129
130 Radiometric ages, precise GPS elevations and stratigraphic de-
131 scriptions of cross-sections surveyed along the Camarones High
132 Terrace are the subject of this paper. Along this terrace, we
133 surveyed and dated samples from two sites, separated by less
134 than one kilometer. One is the *Roadcut*, already recognized
135 and described by Feruglio³⁸. We did not find reports of the
136 second site (that we here call *Caprock*, Figure 1b) in the exist-
137 ing literature, although it is possible that it was included in the
138 geological description of the High Terrace by previous authors.
139 At both sites, we recognized a geological facies representative
140 of sedimentation in a foreshore environment (i.e. in the inter-
141 tidal zone) that marks paleo RSL with high accuracy. All data
142 described hereafter and in Supplementary Note 2 is available in
143 spreadsheet form from Rovere et al. (2020)⁴⁰

144 **Paleo RSL.** In general, *Roadcut* and *Caprock* represent sedi-
145 mentation during a transgressive event on top of a raised shore
146 platform (Supplementary Figure 1-2). Among the units iden-
147 tified within the *Roadcut* (Figure 2), one (Unit **Cp**, see inset
148 in Figure 2) is composed of well-cemented fine conglomerates
149 with rounded pebbles and shells. In particular, the uppermost
150 part of this unit contains a dense faunal assemblage in the form
151 of a shellbed, where we recognized 15 different species of bi-
152 valves and 11 species of gastropods (Supplementary Table 2).
153 The bivalve shells are mostly intact and sometimes with paired
154 valves (articulated), but not in living position. This unit was
155 interpreted as representative of a foreshore environment, i.e. the
156 intertidal zone. The same unit has been identified at the *Caprock*
157 section, at roughly the same elevation. The elevation of Unit
158 **Cp** was measured at two points at both *Roadcut* and *Caprock*

(Table 1). From these measurements, we calculate that Unit **Cp** has an **average elevation of $36.2 \pm 0.9\text{m}$ (1σ)** above the GEOIDEAR16 geoid⁴¹, which is the best approximation for present sea level in Argentina. Using modern tidal values³⁷, and assuming no post-depositional movement, we calculate that the two outcrops in the area of Camarones are indicative of a **paleo RSL at $36.2 \pm 2.7\text{m}$ (1σ)** above present (see Methods for details).

Age. Three oyster shells from *Roadcut* and *Caprock* were analyzed by strontium isotope stratigraphy (SIS) relative dating techniques. Using sequential leaching to target the least altered inner carbonate of each shell, we obtained multiple SIS ages on three different shells (one from *Caprock* and two from *Roadcut*; see Sandstrom et al., 2020¹¹ for a detailed description of the adopted methodology). The shells yielded an age range of **4.69–5.23Ma** ($n=6$, 2σ S_{EM}).

Glacial Isostatic Adjustment. The Early Pliocene intertidal units surveyed at Camarones were subject to processes that caused their past and current elevation to depart from GMSL. These include glacial isostatic adjustment (GIA) and other vertical land motions (VLMs). We calculate GIA using 36 different Earth models. For this site, we calculate a GIA correction of $-14.6 \pm 3.2\text{m}$ (1σ) (see Methods for details). This value is subtracted from the observed paleo RSL and the uncertainty propagated. This correction is a combination of effects associated with i) the ongoing response to the last deglaciation, and ii) Antarctic ice sheet oscillations during the early Pliocene². The former contribution is $-9.5 \pm 3\text{m}$ (1σ), which means that the Argentinian coast today experiences sea level fall due to a combination of effects associated with postglacial rebound due to the melting of the glacial Patagonian ice sheet as well as continental levering, ocean syphoning, and rotational effects. Once fully relaxed, sea level at Camarones will therefore be lower (and a paleo sea level indicator higher) by approximately 9.5m than it is today. The additional contribution of $\sim -5\text{m}$ is associated with the adjustment to 40kyr oscillations in the Antarctic ice sheet. The result is that, at Camarones, **GIA-corrected paleo RSL is $50.8 \pm 4.2\text{m}$ (1σ)**.

Vertical Land Motions. The GIA-corrected RSL elevation reported above needs to be further corrected for VLMs, that can be either due to crustal tectonics, mantle dynamic topography^{42;43} or deformation associated with sediment loading/unloading^{44;45}. As briefly outlined in the previous sections, Camarones is located on a passive margin, likely subject to limited tectonic influence. Dynamic topography models suggest that, since MIS 5e (125 ka), the area of Camarones was subject to uplift, with rates increasing towards the South³. This is in line with observations of much higher Pliocene shorelines (70–170m above sea level³⁶) at locations 300–500 kilometers south of Camarones (Supplementary Note 1). A long-term slight uplift trend is also predicted by the models of Flament et al. (2015)⁴⁶ and Müller et al. (2018)⁴⁷. Predictions in these DT models average to $4.5 \pm 2.2\text{m/Ma}$ (Table 3). Accounting for the age of the deposit (including 1σ uncertainties), this leads to a downward correction of our global mean sea level inference by $22.4 \pm 11.0\text{m}$ (1σ). As is apparent from the variation of estimates for the dynamic topography rate, this correction remains quite uncertain and the true value can possibly be even outside of this range

given that it is difficult to fully explore model uncertainties (see Discussion section).

Global Mean Sea Level. Using the value of VLM reported above and propagating the uncertainties related to RSL, GIA and VLM, we calculate that, at the time of deposition of the *Caprock* and *Roadcut* outcrops, **GMSL was $28.4 \pm 11.7\text{m}$ (1σ)**. We remark that there are large unknowns associated with this value. First, as described above, dynamic topography remains a process that has high uncertainties that are generally not fully quantified. Second, it is possible that, as it is the case for the US Atlantic Coastal Plain⁴⁴, flexural response to sediment loading or tectonic deformation (that are not considered here) could also contribute to further vertical land motions in this area.

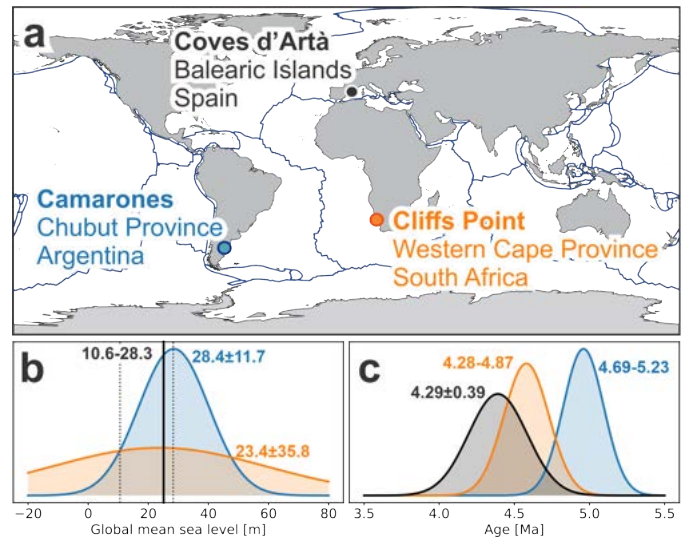


Figure 3: Comparison among Early Pliocene sea level stratigraphic reconstructions. **a)** Location of Early Pliocene RSL indicators discussed in the text. Plate boundaries are shown in dark blue for reference⁴⁸. **b)** Global Mean Sea Level (GMSL) estimates for: i) Coves d'Artà (Balearic Islands, Spain), solid black line represents the most likely value (25.1m), dotted black lines the 16th and 84th percentiles⁹; ii) Camarones, Argentina (blue gaussian); iii) Cliffs Point, South Africa (orange gaussian, calculated from data in Hearty et al. (2020)¹⁰, corrected with the same GIA and subset of applicable DT models used for Camarones. **c)** Age estimates for Coves d'Artà (black), Camarones (blue) and Cliffs Point (orange).

DISCUSSION: EARLY PLIOCENE GLOBAL MEAN SEA LEVEL

Our results show that the intertidal units at Camarones are of Early Pliocene age (4.69–5.23Ma, 2σ S_{EM}). The sedimentological and stratigraphic characteristics of the deposits analysed in this study lead to the conclusion that they formed during a sea level highstand, when GMSL was $28.4 \pm 11.7\text{m}$ (1σ) higher than present. We note that there are still large uncertainties on this GMSL estimate, which derive mostly from vertical land motion corrections, stemming from the variability of published dynamic topography predictions^{46;47}. Exploring and reducing these uncertainties requires improved mapping of the mantle

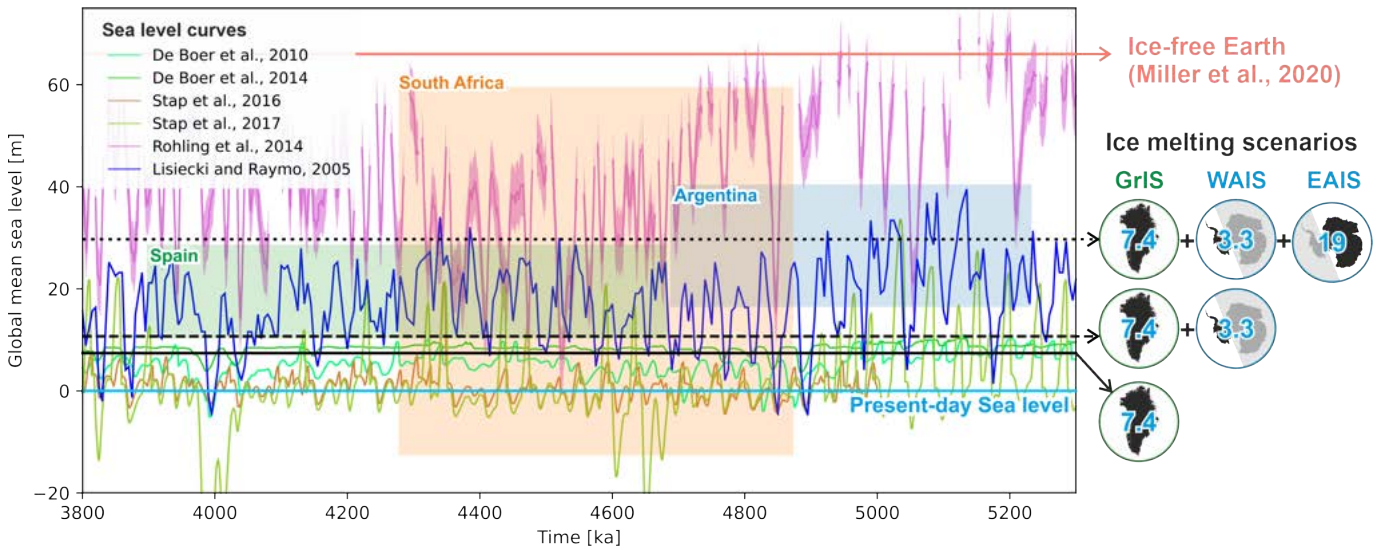


Figure 4: Comparison between sea-level data discussed in this study and global mean sea level derived from ice models^{49;50;51;52} and indirect sea level proxies^{13;53}. The blue curve shows the GMSL prediction that is used in the GIA model and based on scaling the benthic oxygen isotope record by Lisiecki and Raymo (2005)⁵³ following the steps described in the methods. Age ranges for observations are 2σ , while elevation ranges are 1σ for Argentina and South Africa, and 16th-84th percentiles for Spain. Horizontal black lines and graphics on the right side of the graph show total sea level equivalent for ice-free Greenland (GrIS, solid line⁵⁴), melting of West Antarctic Ice Sheet (WAIS, dashed line⁵⁵) and marine sectors of the East Antarctic Ice Sheet (EAIS, dotted line⁵⁶). The upper red line shows GMSL in an ice-free Earth, estimated to 66m by Miller et al. (2020)¹⁵.

241 structure beneath Patagonia from seismic tomography, a better
 242 understanding of how wave speeds map into density variations,
 243 and improved constraints on the rheology of the subsurface. Re-
 244 cent advances tackle these shortcomings and promise to reduce
 245 uncertainties in the estimate of vertical land motion^{57;58}. An-
 246 other strategy to investigate vertical land motions at Camarones
 247 would be to use the Pleistocene shorelines at the same site to
 248 extract a long-term uplift rate for the area. We argue that such
 249 approach would lead to similarly large error bars due to uncer-
 250 tainties related to GIA, Pleistocene global mean sea level and the
 251 implicit assumption that uplift rates can be linearly extrapolated
 252 over these time scales⁵⁹.

253 Despite the uncertainties related to VLMs, there is overlap be-
 254 tween the calculated global mean sea levels for Camarones
 255 ($28.4 \pm 11.7\text{m}$, 1σ) and Coves d' Artá (Spain⁹, 25.1m , with 16th-
 256 84th percentiles of 10.6-28.3m, Figure 3a,b). Correcting the
 257 proxy record at Cliffs Point (South Africa¹⁰) with the same GIA
 258 models used for Camarones (Table 2), results in a paleo RSL
 259 of $44.7 \pm 2.7\text{m}$ (1σ) above present. The DT model predictions
 260 by Müller et al. (2018)⁴⁷, which were also used for Camarones,
 261 indicate VLMs in the range of $4.6 \pm 7.8\text{m/Ma}$ (1σ). This results
 262 in an average global mean sea level estimate that aligns with
 263 those obtained from the other two sites, but bounded by very
 264 large uncertainties ($23.4 \pm 35.8\text{m}$, 1σ), Figure 3b). As already
 265 underlined by Hearty et al. (2020)¹⁰, improving uplift estimates
 266 for this region is paramount to enable the use of RSL data in
 267 GMSL calculations.

268 The average global mean sea level calculated from the geolog-
 269 ical facies reported in Argentina (this study), South Africa¹⁰
 270 and Spain⁹ is well above modern sea level. Compared to pub-
 271 lished global mean sea level estimates that are based on ice

sheet models and indirect sea-level proxies (Figure 4), it is evi-
 272 dent that field evidence is most consistent with the highstands
 273 obtained by scaling the Lisiecki and Raymo (2004)⁵³ benthic
 274 oxygen isotope stack (see Methods for details). Our data is also
 275 consistent with some peaks predicted by the one-dimensional
 276 ice sheet model of Stap et al. (2017)⁵². Other ice sheet model
 277 based estimates^{49;50;51} significantly under predict the observed
 278 Early Pliocene sea level records presented here. The almost-
 279 continuous Gibraltar record¹³, derived from planktic $\delta^{18}\text{O}$ coupled
 280 with a hydraulic model, largely over predicts sea level
 281 observed at both Argentina and Spain suggesting that, when the
 282 Camarones outcrop was deposited, the Earth was substantially
 283 ice-free. To align with this record, the three sites in this study
 284 would have to be characterized by marked subsidence, instead
 285 of uplift as indicated by almost all dynamic topography models
 286 we considered. Early Pliocene observations from Argentina only
 287 overlap with lowstands of the Gibraltar record, which would
 288 have left regressive imprints. This is at odds with the sedi-
 289 mentological characteristics of the *Roacut*, which represents a
 290 transgressive system rather than a regressive one.
 291

292 While GMSL estimates from South Africa¹⁰ are affected by
 293 large uncertainties, their average value together with the Arg-
 294 entinian sea-level proxies presented in this study and those
 295 obtained from Spain⁹, suggest that Early Pliocene GMSL might
 296 have exceeded 20m above present-day levels. Reaching the av-
 297 erage GMSL calculated for Camarones (28.4m) would require
 298 an ice-free Greenland (GrIS, 7.4m sea-level equivalent⁵⁴), sig-
 299 nificant melting of the West Antarctic Ice Sheet (WAIS, 3.3m
 300 sea-level equivalent⁵⁵) and the almost complete melting of mar-
 301 ine sectors of the East Antarctic Ice Sheet (EAIS, 19m sea-level
 302 equivalent⁵⁶). Reaching the lower end calculated for Camarones

303 (16.7m, 1σ below the mean) would require complete melting
 304 of the GrIS and WAIS, and melting of about 1/3 of the marine-
 305 based sectors of the EAIS. This scenario would match almost
 306 exactly a complete GrIS melting, and a contribution from Antarc-
 307 tica in line with the one modelled by Golledge et al. (2007)⁶⁰.
 308 These authors calculated that the contribution of Antarctica to
 309 GMSL during an Early Pliocene (4.23Ma) interglacial was 8.5m,
 310 sourced primarily from WAIS and the Wilkes subglacial basin of
 311 EAIS. Reaching the upper end calculated for Camarones (40.1m,
 312 1σ above the mean) would require significant contributions of
 313 not only marine-based but also land-based sectors of the EAIS
 314 in addition to melting of the GrIS and WAIS. We note that geo-
 315 logical proxies suggest that a significant melting of land-based
 316 portions of EAIS was unlikely over the past 8 million years⁶¹,
 317 which makes this last scenario less likely.

318 CONCLUSIONS

319 The Early Pliocene world was characterized by global annual
 320 mean temperatures of 2-3°C higher than pre-industrial, and CO₂
 321 levels between 280 and 450 ppm¹⁶. In face of these relatively
 322 small differences in temperature and CO₂, the Earth's climate
 323 was substantially different than today¹⁷, and ice sheets were
 324 significantly smaller. Until recently, field evidence to support
 325 the answer to the question "How high was global mean sea level
 326 in the Early Pliocene?" was elusive. In this study, we show that
 327 independent paleo sea-level indicators of similar age on three
 328 continents result in broadly similar GMSL estimates. While
 329 affected by large uncertainties, stemming mostly from vertical
 330 land motion estimates, they indicate that Early Pliocene sea
 331 level may have exceeded 20m above present-day. This value can
 332 be attained only with a complete melting of the Greenland ice
 333 sheet and significant contributions of Antarctica (also including
 334 marine-based sectors of East Antarctica).

335 The significance of the Early Pliocene and its potential role
 336 as analog for present-day and near-future warming must be
 337 taken into account as the world prepares to meet the "Paris
 338 Agreement"⁶² goals and limit global warming below the 1.5°C
 339 threshold⁶³.

340 METHODS

341 **Elevation measurements and paleo RSL estimates.** We
 342 measured elevations with a differential GPS system (Trimble
 343 ProXRT receiver and Trimble Tornado antenna) equipped to
 344 receive OmniSTAR HP real-time corrections. As per technical
 345 specifications by the service provider, these corrections allow to
 346 measure, in optimal conditions, the elevation of a point with an
 347 accuracy of 0.1-0.6 m (2σ), depending on the survey conditions.
 348 We remark that, while at the *Caprock* outcrop there is a free view
 349 of the sky, at the *Roadcut* satellite reception is hindered by the
 350 vertical cliff face. This could explain, in part, the discrepancy
 351 in the two points collected at this outcrop at relatively short
 352 distance from each other. Data were originally recorded
 353 in geographic WGS84 coordinates and in height above the
 354 ITRF2008 ellipsoid. For each GPS point, we calculated heights
 355 above Mean Sea Level (orthometric height) subtracting from
 356 the measured ITRF2008 ellipsoid height the GEOIDEAR16
 357 geoid height⁴¹. These geoidal elevations are the best available
 358 approximation of mean sea level in this area. GEOIDEAR16

was estimated to have an overall accuracy of 10 cm
 (https://www.ign.gov.ar/NuestrasActividades/Geodesia/Geoide-
 Ar16). The location and elevations of Unit **Cp** at *Roadcut* and
Caprock are reported in Table 1.

From these elevations, we calculate that the average elevation
 (μE) is 36.2m. To calculate the elevation error (σE), we use the
 following formula:

$$\sigma E = \sqrt{\frac{\sum_1^N (\sigma E_p^2 \cdot (p-1)) + p \cdot (\mu E - \mu E_p)^2}{N-1}} \quad (1)$$

Where N is the total number of filtered positions measured by
 the GPS during the survey (439, sum of "Number of filtered
 positions" in Table 1), σE_p is the elevation error for each single
 point, μE_p is the Height above geoid of each single point and
 μE is the average elevation (36.2m) (Table 1). On average, we
 calculate that the elevation of Unit **Cp** is $36.2 \pm 0.9\text{m}$ (1σ).

The Unit **Cp** at the *Roadcut* and *Caprock* sites has been inter-
 preted as forming in the foreshore zone, i.e., in the intertidal
 zone. This means that its indicative meaning⁶⁴ spans from
 Mean Lower Low Water (MLLW) to Mean Higher High Wa-
 ter (MHHW). Based on predicted tidal data for the harbor of
 Camarones, Bini et al. (2018)³⁷ report that the maximum tidal
 range (MHHW to MLLW) in Camarones is 5m. We use this
 value (5m) as the indicative range (IR) for a foreshore deposit in
 our area, and the midpoint between MHHW and MLLW (0m)
 as reference water level (RWL). Then, using the formulas de-
 scribed in Rovere et al. (2016)¹, we calculate paleo RSL and its
 associated uncertainty as follows:

$$RSL = \mu E - RWL \quad (2)$$

$$\sigma RSL = \sqrt{\sigma E^2 + \left(\frac{IR}{2}\right)^2} \quad (3)$$

Using the equations above, we calculate that paleo RSL associ-
 ated with Unit **Cp** is $36.2 \pm 2.7\text{m}$. We highlight that this value
 does not take into account the possibility that, 5 Ma ago, tidal
 ranges were different than present-day ones, due to different
 shelf bathymetry under higher sea levels⁶⁵.

To calculate global mean sea level (GMSL) and associated un-
 certainties, we used the following formulas:

$$GMSL = RSL - \mu GIA - \mu VLM \quad (4)$$

Where μGIA is the average of the GIA models (Table 2) and
 μVLM is calculated as the product of mean dynamic topography
 rate (Table 3) multiplied by the average age of the deposit.

$$\sigma GMSL = \sqrt{\sigma RSL^2 + \sigma GIA^2 + \sigma VLM^2} \quad (5)$$

Where σGIA is the standard deviation of GIA models shown in
 Table 2 and σVLM is calculated as follows:

$$\sigma VLM = |VLM| \cdot \sqrt{\left(\frac{\sigma Age}{\mu Age}\right)^2 + \left(\frac{\sigma Rate}{\mu Rate}\right)^2} \quad (6)$$

Table 1: GPS position and elevation of Unit **Cp** measured at the *Roadcut* and *Caprock* sites. Lat/Lon are in WGS84 coordinates, Ellipsoid heights are referred to the ITRF08 ellipsoid, geoid heights to the GEOIDEAR16 geoid model.

Longitude (decimal degrees E)	Latitude (decimal degrees N)	Ellipsoid Height (m)	Height above geoid (μE_p) (m)	Elevation error (σE) (m)	Number of filtered positions (p)
Roadcut					
-65.727604	-44.790083	49.67	36.8	0.06	27
-65.727619	-44.790069	47.68	34.8	0.28	134
Caprock					
-65.728221	-44.799297	49.40	36.5	0.17	249
-65.728221	-44.799298	49.64	36.8	0.12	29
Average			36.2		

396 Where μAge and σAge are the average and 1σ age of the deposit,
 397 and $\mu Rate$ and $\sigma Rate$ are the average and 1σ rates derived from
 398 published dynamic topography models (Table 3).

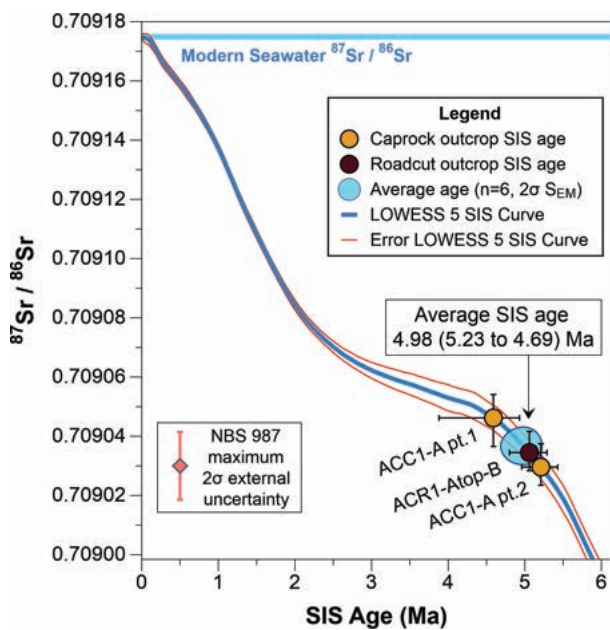


Figure 5: Sr isotope stratigraphy relative ages of oyster shells plotted on the SIS curve (LOWESS version 5) ⁶⁶. Orange points are from two separate portions of a shell from the *Caprock*, while maroon point is of a shell from unit **Cp** in the *Roadcut*. The average SIS age based on these samples is shown as a blue ellipse. Only inner leaches on the best-preserved specimens are shown. For the full dataset, see Supplementary Note 3 annexed to this paper. Modern seawater $^{87}\text{Sr}/^{86}\text{Sr}$ values shown in light blue line. Maximum 2σ external uncertainty for the Sr isotope external standard NBS 987 is shown as red point for comparison (see Methods for details).

399 **Strontium Isotope Stratigraphy ages.** To attribute an age to
 400 Unit **Cp**, we used the Strontium Isotope Stratigraphy (SIS)
 401 curve published by McArthur et al. (2012) ⁶⁶ (LOWESS version
 402 5). Sr isotope ratios from carbonates are susceptible to post-
 403 depositional alteration, therefore, any significant reworking of
 404 Sr isotopes needs to be detected and discarded. Information on
 405 shell preservation was determined using $^{87}\text{Sr}/^{86}\text{Sr}$ measurements

on sequentially leached shell material (assuming smaller Sr iso-
 406 tope variations between leaches implies better preservation ^{67;68})
 407 alongside standard screening techniques ^{36;69} and elemental anal-
 408 ysis ^{70;71}). A preservation index between "1" (unaltered) and
 409 "3" (highly altered) was established for each sample based on
 410 these criteria (Supplementary Note 3, Supplementary Figures
 411 3-7, Supplementary Table 3-4) with samples scoring above "2.0"
 412 excluded from results. The same screening criteria have recently
 413 been used by Hearty et al. (2020) ¹⁰ and are discussed in Sand-
 414 strom et al. (2020) ¹¹. The latter also gives an overview of
 415 the limits and implications of SIS analyses for Plio-Pleistocene
 416 marine samples.
 417

We selected Ostreidae species for SIS chronological constraints,
 418 primarily because these shells precipitate original calcite min-
 419 eral phases, making them more robust to diagenesis than arag-
 420 onitic shells. Sample screening and chemical processing was
 421 carried out at Lamont Doherty Earth Observatory (LDEO), and
 422 all $^{87}\text{Sr}/^{86}\text{Sr}$ measurements were made using Thermal Ion Mass
 423 Spectrometry (TIMS) on an IsotopX Phoenix at SUNY Stony-
 424 brook University (SBU) or a Finnigan Triton Plus at Lamont
 425 Doherty Earth Observatory (LDEO).
 426

We measured three oyster shells, one from the *Caprock* and two
 427 from the *Roadcut* unit. The *Caprock* oyster (ACC1-A) was sam-
 428 pled in three different locations, with inner leaches measured
 429 on two of those splits, returning SIS ages of 4.59Ma (3.88 to
 430 4.93Ma) and 5.21Ma (4.96 to 5.44Ma) (Figure 5). The third
 431 sampling location was only measured for full dissolution, with
 432 an average SIS age of 4.65Ma (4.42 to 4.83Ma), but provided
 433 confidence in the shell Sr isotope heterogeneity and validated
 434 analytical uncertainties. The preservation index score for the
 435 caprock oyster(pt.1) was 1.92. The two shells measured from the
 436 *Roadcut* (ACR1-Atop-B and ACR1-Ctop-C) had inner leach SIS
 437 ages of 5.06Ma (4.80 to 5.28Ma), and 6.35Ma (6.19 to 6.53Ma),
 438 respectively. Additional diagenesis screening techniques on
 439 these shells included elemental analysis (Supplementary Note 3),
 440 and variation of $^{87}\text{Sr}/^{86}\text{Sr}$ within the leach set of each sam-
 441 ple. The results of sample variation compared to the inner leach
 442 $^{87}\text{Sr}/^{86}\text{Sr}$ are shown in the Supplementary Note 3, with low Sr
 443 isotope variation indicative of better preservation. Samples with
 444 low variation tend to exhibit more radiogenic $^{87}\text{Sr}/^{86}\text{Sr}$ values.
 445 Sample ACR1-Atop-B had a preservation index of 1.56, while
 446 ACR1-Ctop-C had a score of 2.33 (Supplementary Table 3).
 447 Based on these screening criteria, we exclude sample ACR1-
 448 Ctop-C, which appeared to have been altered by low $^{87}\text{Sr}/^{86}\text{Sr}$
 449

450 fluids (possibly of through leaching of surrounding volcanic
451 material from the Complejo Marifil³⁹). The remaining inner
452 leaches that passed screening were averaged by filament to ob-
453 tain an age of $4.98 \pm 0.245/-0.295$ Ma ($n=6$, $2\sigma S_{EM}$). In the text,
454 this age is reported as a 2σ range, i.e., 4.69-5.23 Ma.

455 **Glacial Isostatic Adjustment.** To account for changes in ver-
456 tical displacement and gravity field caused by GIA we use a
457 gravitationally self-consistent sea level model, that accounts
458 for the migration of shorelines and feedback of Earth’s rota-
459 tion axis⁷². We compute both the contribution to GIA from
460 the amount of residual deformation caused by the most recent
461 Pleistocene glacial cycles and from ice age cycles during the
462 Pliocene.

463 For the first contribution we use the results from Raymo et al.
464 (2011)², who calculated the residual deformation associated
465 with the ice model ICE-5G⁷³. This ice history is paired with
466 a suite of 36 different earth models with varying lithospheric
467 thickness (48km, 71km, and 96km), upper and lower mantle
468 viscosities (3×10^{20} and 5×10^{20} Pa s for the upper mantle, and
469 3×10^{21} - 30×10^{21} for the lower mantle) to calculate a mean and
470 standard deviation in residual deformation (Figure 6).

471 For the second contribution we follow the approach described
472 in Dumitru et al. (2019)⁹ by estimating ice mass variability
473 based on the benthic stack⁵³. Following Miller et al. (2012)⁷⁴
474 we prescribe that 75% of the benthic $\delta^{18}O$ variability is due to
475 ice volume changes (the rest being due to temperature) and a
476 further scaling of $0.11\text{‰}/10\text{m}$ to convert $\delta^{18}O_{seawater}$ into ice
477 volume changes. These conversions are highly uncertain^{75;76},
478 which highlights the need to obtain local sea level based ice
479 volume estimates. Nonetheless, this scaling was used because
480 it yielded comparable ice volume estimates to the results of
481 Dumitru et al. (2019)⁹. To construct an ice history following
482 this ice volume curve we only assume changes in Antarctic ice
483 volume given evidence that continent wide expansion of northern
484 hemisphere ice sheets did only start around 3.3 Ma⁷⁷. However,
485 we acknowledge that an earlier intermittent Greenland ice sheet
486 might have existed⁷⁸. We compute glacial isostatic adjustment
487 using this ice history and the same suite of 36 different earth
488 models described above. We extract local predictions of relative
489 sea level for Argentina, Mallorca, and South Africa. To calculate
490 global mean sea level changes we integrate the amount of water
491 in the ocean basins as a function of time. We next calculate how
492 this quantity has changed relative to the initial state and divide
493 it by the oceanic area calculated at each time.

494 Note that this setup to calculate the GIA correction deviates
495 slightly from the one described in Dumitru et al.(2019)⁹ in three
496 small ways, (1) we only consider one GMSL history for the
497 Pliocene rather than a range of histories, (2) we only consider
498 variability in southern hemisphere ice sheets and (3) we cal-
499 culated GMSL as described above rather than as changes in
500 grounded ice volume.

501 The GIA corrections from both processes are combined. In a
502 last step we consider the age range for each sea level indicator
503 and average the GIA correction during warm periods, which we
504 define as times that had higher than average sea level over this
505 time period⁹. The mean and standard deviation that is obtained
506 is shown in Table 2. We also show the GIA correction calculated
507 by Dumitru et al. (2019)⁹ and note that the difference in mean

GIA estimates stems mostly from our different definition of
global mean sea level. For the analysis in the main text we use
the GIA correction described in Dumitru et al. (2019)⁹ for the
datapoint from Mallorca and not the one recalculated here.

Table 2: GIA correction for Pliocene sea level markers at the
three locations discussed in the text. For comparison, we also
report the results for Mallorca used in Dumitru et al.⁹.

Location	Longitude	Latitude	μGIA (m)	σGIA (m)
Argentina	65.73° E	44.79° S	-14.6	3.2
South Africa	18.12° W	31.59° S	-9.6	1.6
Mallorca	3.45° W	39.66° N	2.9	2.2
Mallorca ⁹	3.45° W	39.66° N	1.3	3.1

512 **Vertical Land Motions.** VLMs were extracted from pub-
513 lished Dynamic Topography models^{46;47}. The values extracted
514 are reported in Table 3. Flament et al. (2015)⁴⁶ focus on the
515 surface expression of subduction dynamics in South America.
516 Their results are based on forward advection modeling with
517 different tectonic surface boundary conditions. The different
518 cases are based on different timings of slab flattening. Müller
519 et al. (2018)⁴⁷ have a global focus and combine back advect-
520 ion (initialized with a seismic tomography model) and forward
521 advection with tectonic surface boundary conditions. Their dif-
522 ferent models are based on different surface plate reconstructions
523 and different viscosity profiles.

Table 3: Amount of Vertical Land Motion (VLM) at Camarones
from two different studies. Predictions are given at the time step
closest to the sea level indicator age, which is denoted as ‘Tim-
ing’. Rates are calculated based on this age and the predicted
VLM and linearly interpolated to the age of the indicator.

Reference	Model	VLM (m)	Timing (Ma)	Rate (m/Ma)
Müller et al. (2018) ⁴⁷	M1	4.6	10	0.46
	M2	66.2	10	6.62
	M3	45.0	10	4.50
	M4	58.0	10	5.80
	M5	45.4	10	4.54
	M6	21.8	10	2.18
	M7	25.5	10	2.55
Flament et al. (2015) ⁴⁶	Case 1	35.7	5	7.14
	Case 2	37.6	5	7.52
	Case 3	22.9	5	4.58
	Case 4	18.6	5	3.73

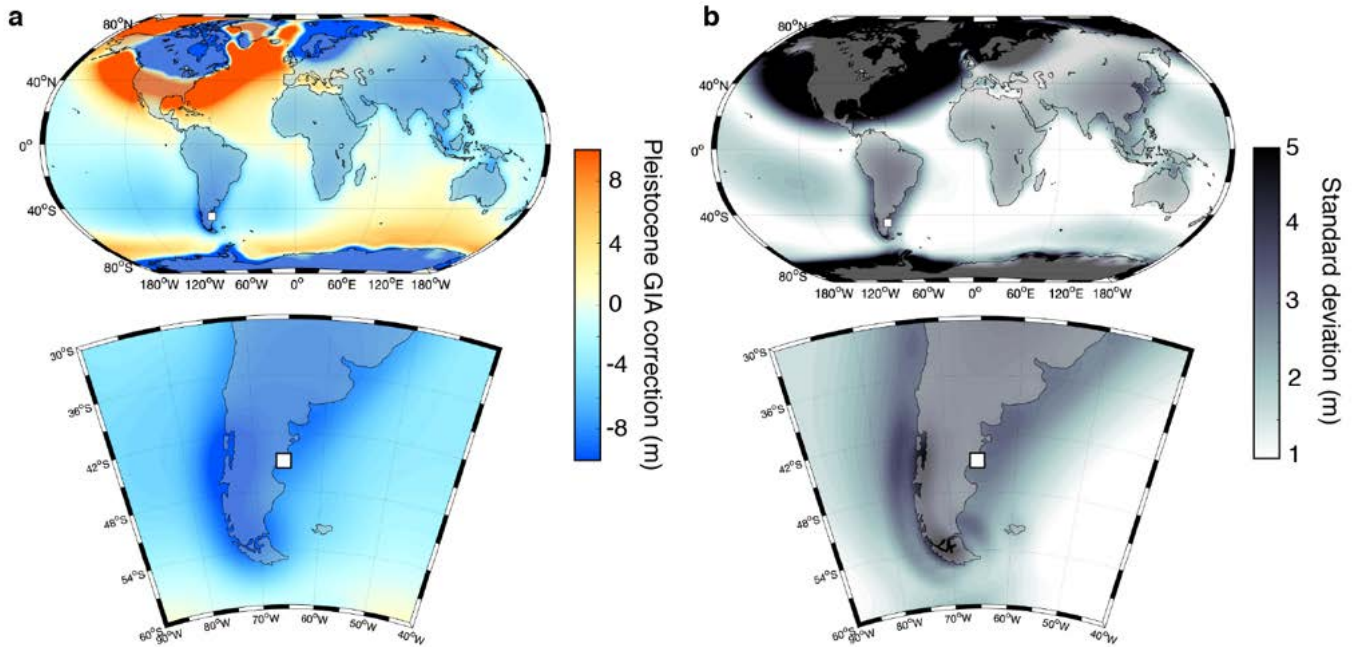


Figure 6: GIA contribution due to ongoing adjustment. The maps show the GIA contribution caused by the incomplete present-day adjustment to the late Pleistocene ice and ocean loading cycles. **a)** Model simulation using a viscosity structure of 5×10^{20} Pa s viscosity in the upper mantle, 5×10^{21} Pa s viscosity in the lower mantle, and an elastic lithospheric thickness of 96 km. **b)** Standard deviation of model predictions obtained using 36 different radial viscosity profiles, including varying the lithospheric thickness. The square in all insets marks the position of Camarones.

524 DATA AVAILABILITY

525 Spreadsheets containing GPS data, GMSL calculations, and
 526 details on shell preservation and ages are available from
 527 <https://doi.org/10.5281/zenodo.3929150>⁴⁰ (CC-BY 4.0 license).
 528 The GEOIDEAR16 geoid model was created by the Insti-
 529 tuto Geográfico Nacional (Ministerio de Defensa, Argentina)
 530 and it was retrieved from the International Service for
 531 the Geoid <http://www.isgeoid.polimi.it/>. Plate boundaries
 532 in Figure 1 and Figure 3 were downloaded from GitHub:
 533 <https://github.com/fraxen/tectonicplates/> (ODC-By license), and
 534 are derived from data by Peter Bird⁴⁸, Hugo Ahlenius and
 535 Nordpil. The background shoreline maps in Figure 3A and
 536 Figure 6 were retrieved from NOAA-NCEI (Global Self-
 537 consistent Hierarchical High-resolution Shoreline, GSHHS⁷⁹).
 538 Equation (1) was derived from a StackExchange discus-
 539 sion ([https://stats.stackexchange.com/questions/25848/how-to-](https://stats.stackexchange.com/questions/25848/how-to-sum-a-standard-deviation)
 540 [sum-a-standard-deviation](https://stats.stackexchange.com/questions/25848/how-to-sum-a-standard-deviation)). Samples described in this study
 541 were registered in the System for Earth Sample Registration
 542 <https://www.geosamples.org/>, and assigned an International Geo-
 543 Sample number (IGSN). Dynamic topography model outputs
 544 were obtained from the Gplates portal (<http://portal.gplates.org/>).

545 CODE AVAILABILITY

546 The python scripts used to produce panels b and c of
 547 Figure 3 and the main panel of Figure 4 are available
 548 from <https://doi.org/10.5281/zenodo.3689426>⁸⁰ (MIT license).
 549 The computer code used to do the sea-level (GIA) cal-

550 culation, written in MATLAB, is available on GitHub
 551 (<https://github.com/jaustermann/SLcode>).

552 ACKNOWLEDGMENTS

553 This research was among the primary objectives of the
 554 PLIOMAX grant, NSF OCE-1202632 (PI MER and co-PI PJH).
 555 AR acknowledges the Institutional Strategy of the University
 556 of Bremen, German Excellence Initiative (ABPZuK-03/2014).
 557 MER and JA acknowledge the additional support of the G. Unger
 558 Vetlesen Foundation. MA acknowledges the following projects:
 559 Agencia Nacional de Promoción Científica y Tecnológica (PICT
 560 2006-468, PICT 2013-1298), CONICET (PIP 0080, 0372 and
 561 0729), and Universidad Nacional de La Plata (PI N11/587 and
 562 N11/726). The authors acknowledge PALSEA for useful dis-
 563 cussions during annual meetings. PALSEA is a working group
 564 of the International Union for Quaternary Sciences (INQUA)
 565 and Past Global Changes (PAGES), which in turn received sup-
 566 port from the Swiss Academy of Sciences and the Chinese
 567 Academy of Sciences. We acknowledge Deirdre Ryan and Evan
 568 Gowan for useful discussions in the field, and Karla Rubio San-
 569 doval Zurisadai for comments on the final draft of the MS. The
 570 background maps in Figure 1 of this article were created using
 571 ArcGIS[®] software by Esri. ArcGIS[®] and ArcMap[™] are the
 572 intellectual property of Esri and are used herein under license.
 573 Copyright[©] Esri. All rights reserved. For more information
 574 about Esri[®] software, please visit www.esri.com.

575 AUTHOR CONTRIBUTIONS

576 AR, MP and SR wrote the MS and supplementary materials,
 577 including figures. SR elaborated the stratigraphic description
 578 of the *Roadcut* outcrop. MA provided expertise on the faunal
 579 composition of the *Roadcut* and *Caprock* outcrops. MRS per-
 580 formed SIS dating and contributed text on SIS methods and
 581 results. JA produced GIA estimates, advised on DT and GMSL
 582 calculations, and contributed to the writing of the paper. PJH
 583 provided expertise on stratigraphic and geological interpretation
 584 on the Camarones outcrops. All authors (except JA) participated
 585 in different phases of the field expeditions to Camarones. IC
 586 identified the *Caprock* site in the field. MER provided expertise
 587 on the paleoclimatic implications of the study. All authors re-
 588 visited the main text and Supplementary Information, and agree
 589 with its contents.

590 COMPETING INTERESTS

591 The authors declare no competing interests

592 REFERENCES

- 593 [1] Rovere, A. *et al.* The analysis of last interglacial (mis 5e)
 594 relative sea-level indicators: Reconstructing sea-level in
 595 a warmer world. *Earth-Science Reviews* **159**, 404–427
 596 (2016).
- 597 [2] Raymo, M. E., Mitrovica, J. X., O’Leary, M. J., DeConto,
 598 R. M. & Hearty, P. J. Departures from eustasy in pliocene
 599 sea-level records. *Nature Geoscience* **4**, 328–332 (2011).
- 600 [3] Austermann, J., Mitrovica, J. X., Huybers, P. & Rovere,
 601 A. Detection of a dynamic topography signal in last inter-
 602 glacial sea-level records. *Science Advances* **3**, e1700457
 603 (2017).
- 604 [4] Dutton, A. *et al.* Sea-level rise due to polar ice-sheet
 605 mass loss during past warm periods. *science* **349**, aaa4019
 606 (2015).
- 607 [5] DeConto, R. M. & Pollard, D. Contribution of antarctica to
 608 past and future sea-level rise. *Nature* **531**, 591–597 (2016).
- 609 [6] Khan, N. S. *et al.* Inception of a global atlas of sea lev-
 610 els since the last glacial maximum. *Quaternary Science*
 611 *Reviews* **220**, 359–371 (2019).
- 612 [7] Pedoja, K. *et al.* Coastal staircase sequences reflecting sea-
 613 level oscillations and tectonic uplift during the quaternary
 614 and neogene. *Earth-Science Reviews* **132**, 13–38 (2014).
- 615 [8] Rovere, A. *et al.* The mid-pliocene sea-level conundrum:
 616 Glacial isostasy, eustasy and dynamic topography. *Earth*
 617 *and Planetary Science Letters* **387**, 27–33 (2014).
- 618 [9] Dumitru, O. A. *et al.* Constraints on global mean sea level
 619 during pliocene warmth. *Nature* **574**, 233–236 (2019).
- 620 [10] Hearty, P. J. *et al.* Pliocene-pleistocene stratigraphy
 621 and sea-level estimates, republic of south africa with
 622 implications for a 400 ppmv co2 world. *Paleoceanography*
 623 *and Paleoclimatology* **35**, e2019PA003835 (2020). URL
 624 [https://agupubs.onlinelibrary.wiley.com/](https://agupubs.onlinelibrary.wiley.com/doi/abs/10.1029/2019PA003835)
 625 doi/abs/10.1029/2019PA003835. E2019PA003835
 626 2019PA003835, [https://agupubs.onlinelibrary.](https://agupubs.onlinelibrary.wiley.com/doi/pdf/10.1029/2019PA003835)
 627 [wiley.com/doi/pdf/10.1029/2019PA003835](https://doi/pdf/10.1029/2019PA003835).
- [11] Sandstrom, M. R. *et al.* Age constraints on surface 628
 deformation recorded by fossil shorelines at Cape 629
 Range, Western Australia. *GSA Bulletin* (2020). URL 630
<https://doi.org/10.1130/B35564.1>. [https://pubs.geoscienceworld.org/gsabulletin/](https://pubs.geoscienceworld.org/gsabulletin/article-pdf/doi/10.1130/B35564.1/5135376/b35564.pdf) 631
[article-pdf/doi/10.1130/B35564.1/5135376/](https://pubs.geoscienceworld.org/gsabulletin/article-pdf/doi/10.1130/B35564.1/5135376/b35564.pdf) 632
[b35564.pdf](https://pubs.geoscienceworld.org/gsabulletin/article-pdf/doi/10.1130/B35564.1/5135376/b35564.pdf). 633
 634
- [12] United States Geological Survey. Shuttle radar topography 635
 mission (SRTM) 1 arc-second global. version 3.0 (2015). 636
- [13] Rohling, E. *et al.* Sea-level and deep-sea-temperature 637
 variability over the past 5.3 million years. *Nature* **508**, 638
 477–482 (2014). 639
- [14] Raymo, M. E., Kozdon, R., Evans, D., Lisiecki, L. & Ford, 640
 H. L. The accuracy of mid-pliocene $\delta 18\text{o}$ -based ice volume 641
 and sea level reconstructions. *Earth-Science Reviews* **177**, 642
 291–302 (2018). 643
- [15] Miller, K. G. *et al.* Cenozoic sea-level and cryospheric 644
 evolution from deep-sea geochemical and continental 645
 margin records. *Science Advances* **6** (2020). URL 646
[https://advances.sciencemag.org/content/6/](https://advances.sciencemag.org/content/6/20/eaaz1346) 647
[20/eaaz1346](https://advances.sciencemag.org/content/6/20/eaaz1346). [https://advances.sciencemag.org/](https://advances.sciencemag.org/content/6/20/eaaz1346.full.pdf) 648
[content/6/20/eaaz1346.full.pdf](https://advances.sciencemag.org/content/6/20/eaaz1346.full.pdf). 649
- [16] Haywood, A. M. *et al.* Are there pre-quaternary geological 650
 analogues for a future greenhouse warming? *Philosophical* 651
Transactions of the Royal Society A: Mathematical, 652
Physical and Engineering Sciences **369**, 933–956 (2011). 653
- [17] Fedorov, A. *et al.* Patterns and mechanisms of early 654
 pliocene warmth. *Nature* **496**, 43–49 (2013). 655
- [18] Lunt, D. J. *et al.* Earth system sensitivity inferred from 656
 pliocene modelling and data. *Nature Geoscience* **3**, 60–64 657
 (2010). 658
- [19] Grant, G. *et al.* The amplitude and origin of sea-level 659
 variability during the pliocene epoch. *Nature* **574**, 237– 660
 241 (2019). 661
- [20] Solgaard, A. M., Reeh, N., Japsen, P. & Nielsen, T. 662
 Snapshots of the greenland ice sheet configuration in the 663
 pliocene to early pleistocene. *Journal of Glaciology* **57**, 664
 871–880 (2011). 665
- [21] Naish, T. *et al.* Obliquity-paced pliocene west antarctic ice 666
 sheet oscillations. *Nature* **458**, 322–328 (2009). 667
- [22] Pollard, D. & DeConto, R. M. Modelling west antarctic 668
 ice sheet growth and collapse through the past five million 669
 years. *Nature* **458**, 329–332 (2009). 670
- [23] Cook, C. P. *et al.* Dynamic behaviour of the east antarctic 671
 ice sheet during pliocene warmth. *Nature Geoscience* **6**, 672
 765–769 (2013). 673
- [24] Dolan, A. M. *et al.* Sensitivity of pliocene ice sheets 674
 to orbital forcing. *Palaeogeography, Palaeoclimatology,* 675
Palaeoecology **309**, 98–110 (2011). 676
- [25] Thomas, C., Livermore, R. & Pollitz, F. Motion of the 677
 scotia sea plates. *Geophysical Journal International* **155**, 678
 789–804 (2003). 679
- [26] Rabassa, J. Late cenozoic glaciations in patagonia and 680
 tierra del fuego. *Developments in quaternary sciences* **11**, 681
 151–204 (2008). 682

- 683 [27] Guillaume, B., Martinod, J., Husson, L., Rod- 740
684 daz, M. & Riquelme, R. Neogene uplift of cen- 741
685 tral eastern patagonia: Dynamic response to ac- 742
686 tive spreading ridge subduction? *Tectonics* **28** 743
687 (2009). URL [https://agupubs.onlinelibrary.](https://agupubs.onlinelibrary.wiley.com/doi/abs/10.1029/2008TC002324)
688 [wiley.com/doi/abs/10.1029/2008TC002324.](https://agupubs.onlinelibrary.wiley.com/doi/pdf/10.1029/2008TC002324)
689 [https://agupubs.onlinelibrary.wiley.com/doi/](https://agupubs.onlinelibrary.wiley.com/doi/pdf/10.1029/2008TC002324)
690 [pdf/10.1029/2008TC002324.](https://agupubs.onlinelibrary.wiley.com/doi/pdf/10.1029/2008TC002324)
- 691 [28] Ton-That, T., Singer, B., Mörner, N.-A. & Rabassa, J. Dat- 744
692 ación de lavas basálticas por 40ar/39ar y geología glacial 745
693 de la región del lago buenos aires, provincia de santa cruz, 746
694 argentina. *Revista de la Asociación Geológica Argentina* **54**, 747
695 333–352 (1999). 748
696 [29] Darwin, C. *Geological observations on South America: 749
697 Being the third part of the geology of the voyage of the 750
698 Beagle, under the command of Capt. Fitzroy, RN during 751
699 the years 1832 to 1836* (Smith, Elder and Company, 65, 752
700 Cornhill., 1846). 753
- 701 [30] Schellmann, G. & Radtke, U. Coastal terraces and 754
702 holocene sea-level changes along the patagonian atlantic 755
703 coast. *Journal of Coastal Research* 983–996 (2003). 756
- 704 [31] Zanchetta, G. *et al.* Middle-to late-holocene relative sea- 757
705 level changes at puerto deseado (patagonia, argentina). *The 758
706 Holocene* **24**, 307–317 (2014). 759
- 707 [32] Pappalardo, M. *et al.* Coastal landscape evolution and 760
708 sea-level change: A case study from central patagonia 761
709 (argentina). *Zeitschrift für Geomorphologie* **59**, 145–172 762
710 (2015). 763
- 711 [33] Rostami, K., Peltier, W. & Mangini, A. Quaternary marine 764
712 terraces, sea-level changes and uplift history of patagonia, 765
713 argentina: comparisons with predictions of the ice-4g 766
714 (vm2) model of the global process of glacial isostatic ad- 767
715 justment. *Quaternary Science Reviews* **19**, 1495–1525 768
716 (2000). 769
- 717 [34] Schellmann, G. & Radtke, U. ESR dating stratigraphically 770
718 well-constrained marine terraces along the patagonian atl- 771
719 antic coast (argentina). *Quaternary International* **68**, 261– 772
720 273 (2000). 773
- 721 [35] Rutter, N. *et al.* Correlation and dating of quaternary 774
722 littoral zones along the patagonian coast, argentina. *Qua-* 775
723 *ternary Science Reviews* **8**, 213–234 (1989). 776
- 724 [36] Del Río, C., Griffin, M., McArthur, J., Martínez, S. & 777
725 Thirlwall, M. Evidence for early pliocene and late miocene 778
726 transgressions in southern patagonia (argentina): 87sr/86sr 779
727 ages of the pectinid "chlamys" actinodes (sowerby). *Journal of South American Earth Sciences* **47** (2013). 780
728
- 729 [37] Bini, M. *et al.* Mid-holocene relative sea-level changes 781
730 along atlantic patagonia: new data from camarones, chubut, 782
731 argentina. *The Holocene* **28**, 56–64 (2018). 783
- 732 [38] Feruglio, E. *Descripción geológica de la Patagonia*, vol. 1 784
733 (Impr. y Casa Editora "Coni", 1949). 785
- 734 [39] Lema, H. A. *et al.* *Hoja Geológica 4566-II y IV Camarones* 786
735 (Servicio Geológico Minero Argentino. Instituto de Ge- 787
736 ología y Recursos Minerales, 2001). 788
- 737 [40] Rovere, A. *et al.* Survey data, models and dated samples of 789
738 the pliocene shorelines of camarones, argentina (ver 1.1). 790
739 (2020). 791
- [41] Piñón, D., Zhang, K., Wu, S. & Cimbaro, S. A new argen- 792
tinean gravimetric geoid model: Geoidear. In *International 793
Symposium on Earth and Environmental Sciences for Future 794
Generations*, 53–62 (Springer, 2017). 795
- [42] Braun, J. The many surface expressions of mantle dynam- 796
ics. *Nature Geoscience* **3**, 825–833 (2010). 797
- [43] Moucha, R. *et al.* Dynamic topography and long-term 798
sea-level variations: There is no such thing as a stable 799
continental platform. *Earth and Planetary Science Letters* **271**, 101–108 (2008). 800
- [44] Moucha, R. & Ruetenik, G. A. Interplay between dynamic 801
topography and flexure along the us atlantic passive margin: 802
Insights from landscape evolution modeling. *Global and 803
Planetary Change* **149**, 72–78 (2017). 804
- [45] Ferrier, K. L., Austermann, J., Mitrovica, J. X. & Pico, T. 805
Incorporating sediment compaction into a gravitationally 806
self-consistent model for ice age sea-level change. *Geo-* 807
physical Journal International **211**, 663–672 (2017). 808
- [46] Flament, N., Gurnis, M., Müller, R. D., Bower, D. J. & 809
Husson, L. Influence of subduction history on south amer- 810
ican topography. *Earth and Planetary Science Letters* **430**, 811
9–18 (2015). 812
- [47] Müller, R. D., Hassan, R., Gurnis, M., Flament, N. & 813
Williams, S. E. Dynamic topography of passive conti- 814
nental margins and their hinterlands since the Cretaceous. 815
Gondwana Research **53**, 225–251 (2018). 816
- [48] Bird, P. An updated digital model of plate boundaries. 817
Geochemistry, Geophysics, Geosystems **4** (2003). 818
- [49] De Boer, B., Van de Wal, R., Bintanja, R., Lourens, L. & 819
Tuenter, E. Cenozoic global ice-volume and temperature 820
simulations with 1-d ice-sheet models forced by benthic δ 821
18 o records. *Annals of glaciology* **51**, 23–33 (2010). 822
- [50] De Boer, B., Lourens, L. J. & Van De Wal, R. S. Persistent 823
400,000-year variability of antarctic ice volume and the 824
carbon cycle is revealed throughout the plio-pleistocene. 825
Nature Communications **5**, 2999 (2014). 826
- [51] Stap, L. B. *et al.* CO₂ over the past 5 million years: Con- 827
tinuous simulation and new δ 11b-based proxy data. *Earth 828
and Planetary Science Letters* **439**, 1–10 (2016). 829
- [52] Stap, L. B., Van De Wal, R. S., De Boer, B., Bintanja, 830
R. & Lourens, L. J. The influence of ice sheets on tem- 831
perature during the past 38 million years inferred from a 832
one-dimensional ice sheet-climate model. *Climate of the 833
Past* **13**, 1243–1257 (2017). 834
- [53] Lisiecki, L. E. & Raymo, M. E. A pliocene-pleistocene 835
stack of 57 globally distributed benthic δ 18o records. *Pae-* 836
leoceanography **20** (2005). 837
- [54] Morlighem, M. *et al.* Bedmachine v3: Complete bed top- 838
ography and ocean bathymetry mapping of greenland 839
from multibeam echo sounding combined with mass con- 840
servation. *Geophysical research letters* **44**, 11–051 (2017). 841
- [55] Bamber, J. L., Riva, R. E., Vermeersen, B. L. & LeBrocq, 842
A. M. Reassessment of the potential sea-level rise from 843
a collapse of the west antarctic ice sheet. *science* **324**, 844
901–903 (2009). 845

- 795 [56] Fretwell, P. *et al.* Bedmap2: improved ice bed, surface 852
796 and thickness datasets for antarctica. *The Cryosphere* **7**, 853
797 375–393 (2013). 854
- 798 [57] Richards, F. D., Hoggard, M. J., White, N. & Ghe- 855
799 lichkhan, S. Quantifying the relationship between 856
800 short-wavelength dynamic topography and thermome- 857
801chanical structure of the upper mantle using calibrated 858
802 parameterization of anelasticity. *Journal of Geo-*
803 *physical Research: Solid Earth* **125**, e2019JB019062
804 (2020). URL [https://agupubs.onlinelibrary.](https://agupubs.onlinelibrary.wiley.com/doi/abs/10.1029/2019JB019062)
805 [wiley.com/doi/abs/10.1029/2019JB019062](https://agupubs.onlinelibrary.wiley.com/doi/abs/10.1029/2019JB019062).
806 E2019JB019062 10.1029/2019JB019062, [https://agupubs.onlinelibrary.wiley.com/doi/pdf/](https://agupubs.onlinelibrary.wiley.com/doi/pdf/10.1029/2019JB019062)
807 [10.1029/2019JB019062](https://agupubs.onlinelibrary.wiley.com/doi/pdf/10.1029/2019JB019062). 808
- 809 [58] Lloyd, A. J. *et al.* Decoding cenozoic tectonics in patag-
810 onia, the scotia sea, and the antarctic peninsula from new
811 seismic tomography. *AGUFM* **2019**, T41J–0286 (2019).
- 812 [59] Stocchi, P. *et al.* Mis 5e relative sea-level changes in the
813 mediterranean sea: Contribution of isostatic disequilibrium.
814 *Quaternary Science Reviews* **185**, 122–134 (2018).
- 815 [60] Golledge, N. R. *et al.* Antarctic climate and ice-sheet
816 configuration during the early pliocene interglacial at 4.23
817 ma. *Climate of the Past* **13** (2017).
- 818 [61] Shakun, J. D. *et al.* Minimal east antarctic ice sheet retreat
819 onto land during the past eight million years. *Nature* **558**,
820 284–287 (2018).
- 821 [62] Rogelj, J. *et al.* Paris agreement climate proposals need
822 a boost to keep warming well below 2 c. *Nature* **534**,
823 631–639 (2016).
- 824 [63] IPCC. *Global warming of 1.5 C. An IPCC Special Re-*
825 *port on the impacts of global warming of 1.5 C above*
826 *pre-industrial levels and related global greenhouse gas*
827 *emission pathways, in the context of strengthening the*
828 *global response to the threat of climate change, sustain-*
829 *able development, and efforts to eradicate poverty* (2018).
- 830 [64] Shennan, I. Flandrian sea-level changes in the fenland. ii:
831 Tendencies of sea-level movement, altitudinal changes, and
832 local and regional factors. *Journal of Quaternary Science*
833 **1**, 155–179 (1986).
- 834 [65] Green, J., Huber, M., Waltham, D., Buzan, J. & Wells,
835 M. Explicitly modelled deep-time tidal dissipation and its
836 implication for lunar history. *Earth and Planetary Science*
837 *Letters* **461**, 46–53 (2017).
- 838 [66] McArthur, J., Howarth, R. & Shields, G. Strontium isotope
839 stratigraphy. *The geologic time scale* **1**, 127–144 (2012).
- 840 [67] Bailey, T., McArthur, J., Prince, H. & Thirlwall, M. Dissol-
841 ution methods for strontium isotope stratigraphy: whole
842 rock analysis. *Chemical Geology* **167**, 313–319 (2000).
- 843 [68] Li, D., Shields-Zhou, G. A., Ling, H.-F. & Thirlwall, M.
844 Dissolution methods for strontium isotope stratigraphy:
845 Guidelines for the use of bulk carbonate and phosphorite
846 rocks. *Chemical Geology* **290**, 133–144 (2011).
- 847 [69] McArthur, J. M. Recent trends in strontium isotope stratig-
848 raphy. *Terra nova* **6**, 331–358 (1994).
- 849 [70] Brand, U. & Veizer, J. Chemical diagenesis of a multicom-
850 ponent carbonate system; 1, trace elements. *Journal of*
851 *Sedimentary Research* **50**, 1219–1236 (1980).
- [71] Gothmann, A. M. *et al.* Fossil corals as an archive of 852
secular variations in seawater chemistry since the mesozoic. 853
Geochimica et Cosmochimica Acta **160**, 188–208 (2015). 854
- [72] Kendall, R. A., Mitrovica, J. X. & Milne, G. A. On post- 855
glacial sea level–ii. numerical formulation and comparative 856
results on spherically symmetric models. *Geophysical*
857 *Journal International* **161**, 679–706 (2005). 858
- [73] Peltier, W. Global glacial isostasy and the surface of the 859
ice-age earth: the ice-5g (vm2) model and grace. *An-*
860 *nual Review of Earth and Planetary Sciences* **32**, 111–149
861 (2004). 862
- [74] Miller, K. G. *et al.* High tide of the warm pliocene: Im- 863
plications of global sea level for antarctic deglaciation. 864
Geology **40**, 407–410 (2012). 865
- [75] Raymo, M. E., Kozdon, R., Evans, D., Lisiecki, L. & Ford, 866
H. L. The accuracy of mid-pliocene $\delta^{18}O$ -based ice volume 867
and sea level reconstructions. *Earth-Science Reviews* **177**,
868 291–302 (2018). 869
- [76] Gasson, E., DeConto, R. M. & Pollard, D. Modeling the 870
oxygen isotope composition of the antarctic ice sheet and 871
its significance to pliocene sea level. *Geology* **44**, 827–830
872 (2016). 873
- [77] Jansen, E., Fronval, T., Rack, F. & Channell, J. E. T. 874
Pliocene-pleistocene ice rafting history and cyclicity in 875
the nordic seas during the last 3.5 myr. *Paleoceanography*
876 **15**, 709–721 (2000). 877
- [78] Bierman, P. R., Shakun, J. D., Corbett, L. B., Zimmerman, 878
S. R. & Rood, D. H. A persistent and dynamic east green- 879
land ice sheet over the past 7.5 million years. *Nature* **540**,
880 256–260 (2016). 881
- [79] Wessel, P. & Smith, W. H. A global, self-consistent, hi- 882
erarchical, high-resolution shoreline database. *Journal*
883 *of Geophysical Research: Solid Earth* **101**, 8741–8743
884 (1996). 885
- [80] Rovere, A. Paleo sea level utilities (ver 1.5) (2020). 886

HIGHER THAN PRESENT GLOBAL MEAN SEA LEVEL RECORDED BY AN EARLY PLIOCENE INTERTIDAL UNIT IN PATAGONIA (ARGENTINA) - SUPPLEMENTARY INFORMATION -

PREPRINT, COMPILED NOVEMBER 11, 2020

Alessio Rovere^{1*}, Marta Pappalardo², Sebastian Richiano³, Marina Aguirre^{4,5}, Michael R. Sandstrom⁶, Paul J. Hearty⁷, Jacqueline Austermann⁶, Ignacio Castellanos⁵, and Maureen E. Raymo⁶

¹MARUM - Center for Marine Environmental Sciences, University of Bremen. Leobener Str. 8., D-28359, Bremen, Germany

²Department of Earth Sciences, Università degli studi di Pisa. Via S. Maria 53, 56126, Pisa Italy

³Instituto Patagónico de Geología y Paleontología, CONICET. Bv. Almirante Brown 2915, Puerto Madryn (9120), Chubut, Argentina

⁴CONICET, CCT-La Plata and Universidad Nacional de La Plata. Calle 8 n.1467, B1904CMC, La Plata, Buenos Aires, Argentina

⁵Facultad de Ciencias Naturales y Museo, Universidad Nacional de La Plata. Calle 64 n.3, 1900 La Plata, Buenos Aires, Argentina

⁶Lamont Doherty Earth Observatory, Columbia University. 61 Rte 9W, Palisades, NY 10964, United States

⁷Department of Geological Sciences, Jackson School of Geosciences, The University of Texas at Austin. 2275 Speedway Stop C9000, Austin, Texas, United States

1 SUPPLEMENTARY NOTE 1: PALEO RELATIVE SEA LEVEL 2 INDICATORS IN PATAGONIA

marine/beach deposits were recognized from present-day coast-
line inland.

Holocene. Holocene sea level indicators at Camarones mark the maximum sea level transgression and a sequence of regressive beach ridges. Bini et al. (2018)²² reported precisely measured Holocene RSL proxies dated with ¹⁴C, indicating that, between ca. 5300 and 7000 cal. yr BP, RSL was 2 to 4 m above present sea level (elevations referred to the EGM2008 Geoid).

Marine Isotopic Stage 5e. The Last Interglacial is also preserved in the form of relic beach ridges in the Camarones area. These were investigated and dated by different authors throughout the years^{9;12;10;23} (Supplementary Table 1). A recent study by Pappalardo et al. (2015)⁹ provides more precise measurements, interpretations and additional dating of the MIS 5e beach ridge complex at Camarones. According to these authors⁹, the beach ridges at Camarones indicate a MIS 5e paleo RSL at 7.5 ±2/-3.5m above present.

Marine Isotopic Stage 11. At one site south of Camarones town, articulated shells from (Sample Pa 35) was dated by Schellmann and Radtke (2000)¹² as MIS 9 or older. U-series mollusk ages by Pappalardo et al. (2015)⁹ confirm the attribution to MIS 11. We measured the deposits dated by these authors at 16.7 ± 0.4m above present sea level.

SUPPLEMENTARY NOTE 2: DETAILED DESCRIPTION OF *Roadcut* AND *Caprock* UNITS AT CAMARONES

The *Roadcut* section (Supplementary Figure 1) is characterized by the bedrock (*Formación Río Chico*) outcropping from the road level up to ca.12m above it. The topmost part of the bedrock is exposed for a maximum thickness of 1.2m in the western part of the outcrop and it is shaped as a flat, gently eastward (i.e. seaward) dipping platform. All the overlying units are separated from it by a sharp erosional unconformity. Less than 1 km south of the *Roadcut*, another outcrop shows the same geological context. We refer to this as the *Caprock* outcrop

3 The study of paleo shorelines in Patagonia dates back to Charles
4 Darwin, who was the first to provide an account of the coastal
5 stratigraphy in the region¹. Nearly a century later, the Italian ge-
6 ologist Feruglio reported the first full account of marine terraces
7 along the Patagonian coast (Chubut and Santa Cruz Provinces)²,
8 that he grouped into six systems. The two uppermost systems
9 were attributed to the to late Pliocene–early Pleistocene³ based
10 on biostratigraphic features and their high elevation (40-50 and
11 80-95 m asl). Several studies detailed the stratigraphy, elevation
12 and age of Holocene^{4;5}, Pleistocene^{6;7;8;9;10;11;12} and Pliocene-
13 to-Miocene^{13;14} marine and coastal deposits. The Tertiary ma-
14 rine sediments were assigned to Miocene and Pliocene periods
15 mostly on the basis of biostratigraphy. Several authors worked
16 to characterize the Marine Miocene of Patagonia^{15;16;17} and the
17 Mio-Pliocene¹⁸. Concerning the Early Pliocene, a marine de-
18 posit in Northern Patagonia (Rio Negro Province) yielded a
19 fission track age of 4.41 Ma¹⁹, but this age was later considered
20 inconsistent with biostratigraphic characteristics of the deposits
21 and thus rejected²⁰. Del Río et al. (2013)¹⁴ dated samples of
22 mollusks from marine deposits in Central and Southern Patag-
23 onia, few hundreds kilometers south of our study area. The
24 marine deposits of Cerro Laciár (300 km south of the area in-
25 vestigated in this study, 170-185m above MSL) yielded ages of
26 5.10 ± 0.21 Ma, and those of Cañadon Darwin (540 km south of
27 the area investigated by this study, 65-75m above MSL) yielded
28 ages of 5.15 ± 0.18 Ma. These two data points represent the
29 first geochemically constrained evidence of a (Early) Pliocene
30 transgression in the area.

31 In the coastal area around the Camarones town, the main lithos-
32 tratigraphic units are a Jurassic volcanic complex (*Complejo*
33 *Marifil*), and Upper Paleocene sedimentary rocks (*Formación*
34 *Río Chico*)²¹. According to published geological maps²¹, the
35 volcanic complex is composed by reddish rhyolites, leucorhyo-
36 lites and ignimbrites, whereas the Río Chico formation is made
37 of mudstones, sandstones and conglomerates, often volcanoclas-
38 tic. Along the same coastal section, fossil beach ridges and

39
40
41
42
43
44
45
46
47
48
49
50
51
52
53
54
55
56
57
58
59
60
61
62
63
64
65
66
67
68
69
70
71
72

Supplementary Table 1: Ages of beach ridges associated to MIS 5e in the Camarones area.

Location	Author	Sample	Subsample	Age (ka)	Age uncertainty (ka)	Dating technique	
Camarones North IV	Schellmann (1998) ²³	Pa 30	D2412A	117	21	ESR	
			D2635	123	22	ESR	
			K2412B	139	8	ESR	
			D2550	92	9	ESR	
			D2549	99	12	ESR	
Camarones North I	Schellmann (1998) ²³	Pa 47c	D2665	115	9	ESR	
			D2547	117	13	ESR	
			D2546	133	15	ESR	
			D2545	137	18	ESR	
			D2548	144	19	ESR	
Camarones 12km South	Rostami et al., 2000 ¹⁰	3	3-0/1	117	5	U-Series	
			3-0/2	115	9	U-Series	
			3-0/2	110	8	ESR	
			3-0/3	112	13	U-Series	
			3-0/3	114	9	ESR	
Various sites North and south of Camarones	Pappalardo et al., 2015 ⁹	WP64A(3)	N/A	121	0.9	U-Series	
			WP65(1)	N/A	130	2.5	U-Series
			WP68(1)	N/A	131	1.1	U-Series
			WP70(B)	N/A	127	1.2	U-Series

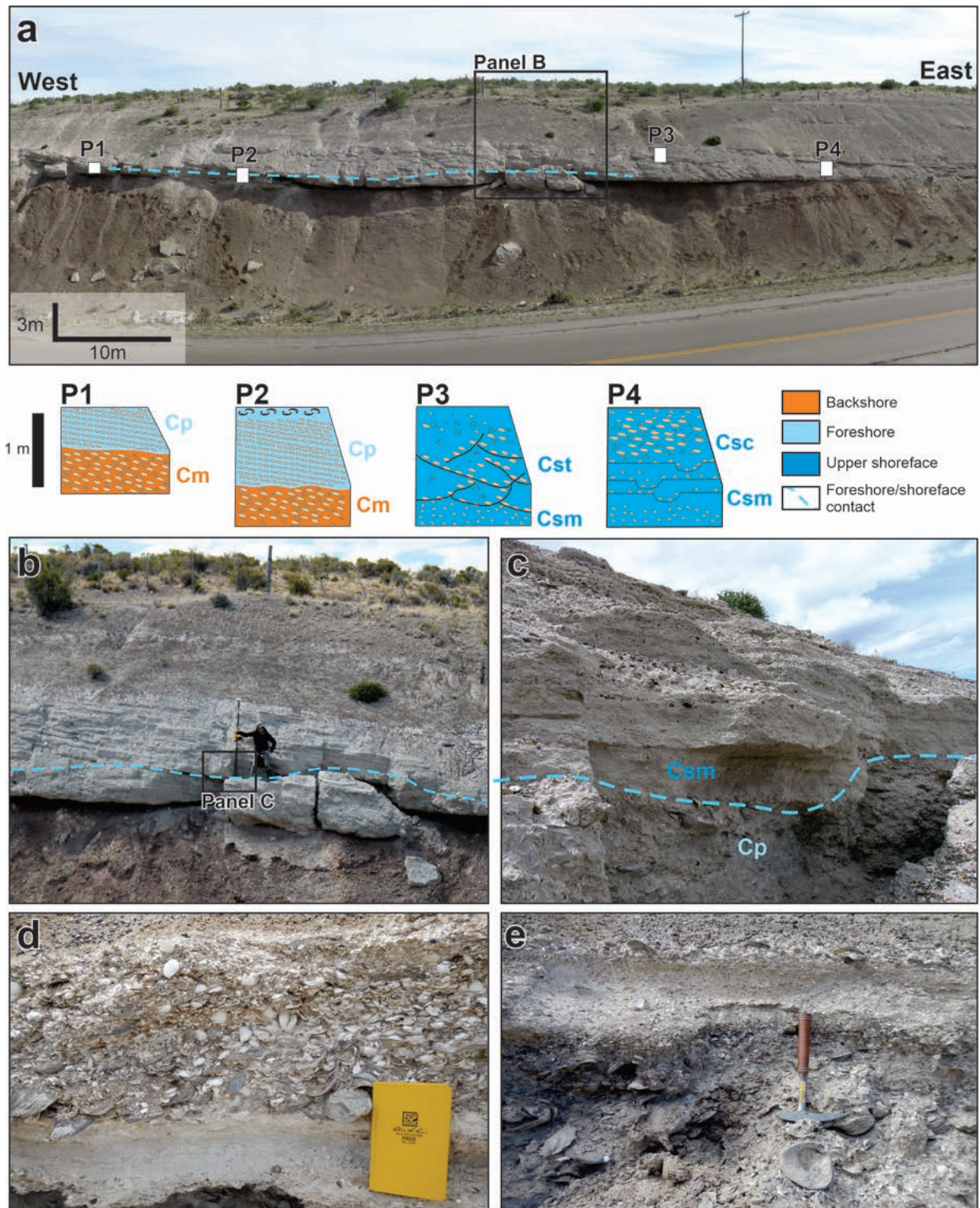
(Supplementary Figure 2). This rests on a relative topographic high of the bedrock, which at this location is represented by the volcanic rocks pertaining to the *Complejo Marifil*, capped by a thin sedimentary unit, as thick as 1m maximum, identical to the upper part of the Cp Unit observed in the *Roadcut* section. Each overlying unit is described separately hereafter.

Unit Cm. In the western part of the section on top of the bedrock rests a basal unit (Cm). This is represented by a massive, clast-supported conglomerate with coarse rounded pebbles of different rock types. Pebbles have an imbricated, seaward dipping bedding. Faunal content is absent.

Unit Cp. Eastward, a finer unit (Cp) overlaps the previous one and, towards the East, unconformably rests on the bedrock. Unit Cp is composed of well-cemented fine conglomerates with rounded pebbles, mostly unbroken shells and abundant sandy matrix, displaying a low-angle planar cross-stratification. The uppermost part of Cp contains a dense faunal assemblage in the form of a shellbed, with different shell types (Supplementary Table 2) mostly intact and sometimes with paired valves (articulated), but not in living position. Only the fragmentation of Pectinids is relevant, which is expected even with minimal transport as they have a fragile shell structure. The shells in Unit Cp are characterized by different stages of preservation, depending mostly on the shell type. Big oysters (*Crassostrea* sp.), up to 15 cm in size, are frequent, mostly oriented concordant with strata dip and strike. They underwent partial dissolution, especially of their outer part, which explains the high degree of cementation of this unit. The faunal assemblage of Unit Cp is analogous to that of the Pleistocene terraces towards the coast, with notable exceptions. The absence of *Tegula atra* (cold gastropod species), together with the occurrence of bivalves of warm/warm-temperate affinity (*C. patagonica*, *D. patagonica*, *F. vilardebona*, *M. cf. isabelleana*), is the main difference relative to the Pleistocene deposits. Cp has a maximum thickness of 1m in the western part of the outcrop (stratigraphic column B, Supplementary Figure 1b).

Unit Cs. East of this point, the Cp unit becomes progressively thinner, and is overlapped by a finer unit (Cs) of matrix-supported sandy conglomerates. The contact between Cp and Cs is planar and displays a lateral continuity up to the midpoint of the section, East of which Cs lays directly on the bedrock. The basal part of Cs is massive (Csm) with no sedimentary structures, whereas its uppermost part, separated from Csm by a gradational contact, displays trough cross-stratification (Cst) and, more eastward, longitudinal channels (Csc).

Overall, this section represents the product of sedimentation due to a transgressive event on top of a marine platform carved in the volcanic bedrock. The sequence is fining (and thus deepening) upward. The similarities of the basal unit (Cm) with modern storm berms in the area suggest that it was formed in a backshore environment. We interpret Unit Cp as the product of sedimentation in a foreshore environment. The bedding of marine shells within this unit testifies that they have been reworked within the surf zone where sediments from upper offshore and shoreface are floated towards the beachface and from there are driven back by rip currents, producing an isorientation of single shells parallel to the current direction. The topmost Units (Csm, Cst and Csc) can be interpreted as mainly developed in middle to upper shoreface. The sedimentary structures within these units can be interpreted as the product of longitudinal currents caused by coastal drift.



Supplementary Figure 1: **a**) General view of the *Roadcut* section. Below the photo, four stratigraphic profiles (P1-P4) detailing the relationships between the main sedimentary facies. **Cm**: Conglomerate, massive; **Cp**: Conglomerate with low angle planar cross-stratification; **Csm**: Sandy conglomerate, massive; **Cst**: Sandy conglomerate with trough cross-stratification; **Csc**: Sandy conglomerate with longitudinal channels. **b**) Location where the elevation of unit **Cp** has been measured (the points listed in the main paper are located near the person standing on the outcrop). **c**) Detail of the contact between **Cp** (foreshore) and **Csm** (upper foreshore). **d**) and **e**) Details of the bivalve-rich horizon sampled for Sr isotopes dating.

Supplementary Table 2: Faunal assemblage in the marine deposits outcropping at the *Roadcut* section at Camarones. Most of the species recognized by Feruglio^{3;2} and assigned to the highest terrace system (that was tentatively dated to Pliocene) were detected in the Cp Unit of the *Roadcut* section (This work). Nomenclature of the taxa has been updated as some generic or specific names do not agree with those used by Feruglio. * indicates species with warm/warm-temperate affinity.

BIVALVIA	Feruglio ^{3;2}	This work
<i>Aulacomya atra</i> (Molina, 1782)	X	X
<i>Aequipecten tehuelchus</i> (d'Orbigny, 1842)	X	
<i>Zygochlamys patagonica</i> (King, 1832)	X	X
<i>Pectinidae</i> indet.		X
<i>Ostrea equestris</i> Say, 1834		X
<i>Ostrea puelchana</i> d'Orbigny, 1842	X	
<i>Ostrea tehuelcha</i> Feruglio	X	X
<i>Ostrea cf. tehuelcha</i> Feruglio		X
<i>Ostrea sp.</i>		X
<i>Ostrea tehuelcha</i> d'Orbigny*		X
<i>Diplodonta patagonica</i> (d'Orbigny, 1842)*		X
<i>Felaniella vilardeboana</i> (d'Orbigny, 1846)*	X	
<i>Diplodonta sp.</i>	X	
<i>Abra sp.</i>		X
<i>Mactra cf. isabellena</i> d'Orbigny, 1846*	X	X
<i>Mactra cf. patagonica</i> d'Orbigny		X
<i>Eurhomalea exalbida</i> (Dilwyn, 1817)		X
<i>Ameghinomya antiqua</i> (King, 1832)		X
<i>Pitar rostratus</i> (Philippi, 1844)	X	X
<i>Corbula patagonica</i> d'Orbigny 1845	X	X
GASTROPODA		
<i>Epitonium georgettinum</i> (Kiener, 1838)	X	X
<i>Trophon varians</i> (d'Orbigny, 1841)	X	X
<i>Trophon geversianus</i> (Pallas, 1774)	X	X
<i>Trophon laciniatus</i> (Martin)	X	X
<i>Adelomelon ancilla</i> (Lightfoot, 1786)	X	X
<i>Adelomelon ferussaci</i> (Donovan, 1824)		
<i>Adelomelon sp.</i>		X
<i>Odontocymbiola magellanica</i> (Gmelin, 1791)	X	X
<i>Olivancillaria auricularia</i> (Lamarck, 1811)	X	X
<i>Olivancillaria cf. carcellesi</i> Klappenbach, 1965		
<i>Buccinanops deformis</i> (P.P. King, 1832)	X	X
<i>Buccinanops cochlidium</i> (Dilwyn, 1817)	X	
<i>Buccinanops sp.</i>	X	X
<i>Siphonaria lessonii</i> Blainville, 1827		
<i>Volutidae</i> indet.	X	X

134 SUPPLEMENTARY NOTE 3: SIS AGE DETAILS.

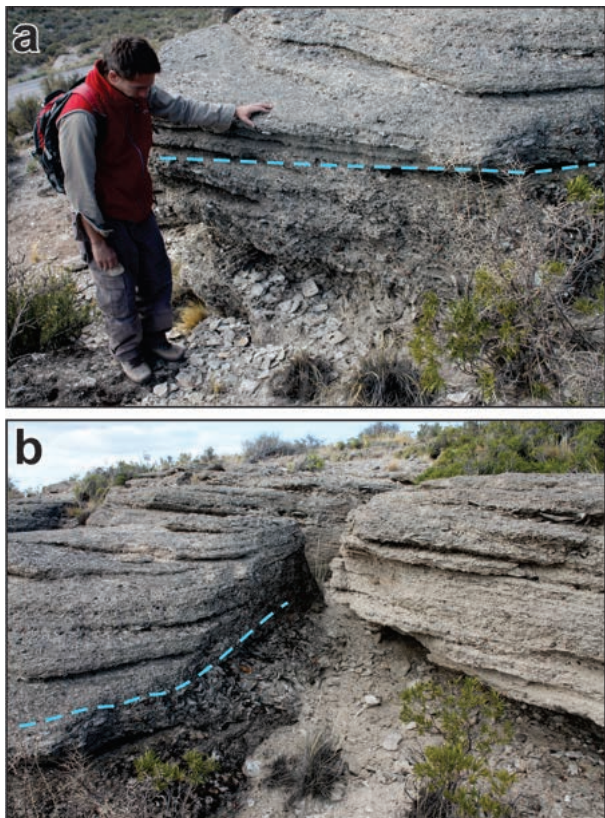
135 Details on samples and SIS analyses performed are shown here-
 136 after, in Supplementary Figures 3 to 7. Full SIS age results are
 137 reported in Supplementary Table 4.

138 Initial field selection criteria involved visual assessment based on
 139 shell thickness, coloration, and diagnostic features of preservation
 140 of original layers, and diagnostic features of preservation, including microborings, Fe and Mg staining, fragmentation
 141 of original layers, and irregularities in structure^{14;24;25} (Sup-
 142 plementary Figure 4. In the laboratory, samples were slabbed,
 143 polished and imaged using an optical microscope with CCD
 144 camera for further inspection. and an ASPEX Express scanning
 145 electron microscope (SEM). This preliminary screening method
 146 helps identify locations of alteration that can be correlated with
 147 the ⁸⁷Sr/⁸⁶Sr leach variations and establishes the overall integrity

of preservation in each shell. A preservation scoring system was
 established as outlined in Hearty et al. (2020)²⁶, with optical
 and SEM images assigned scores from "1" (no visible alteration)
 to "3" (significant alteration observable) based on screening
 criteria above (Supplementary Table 3).

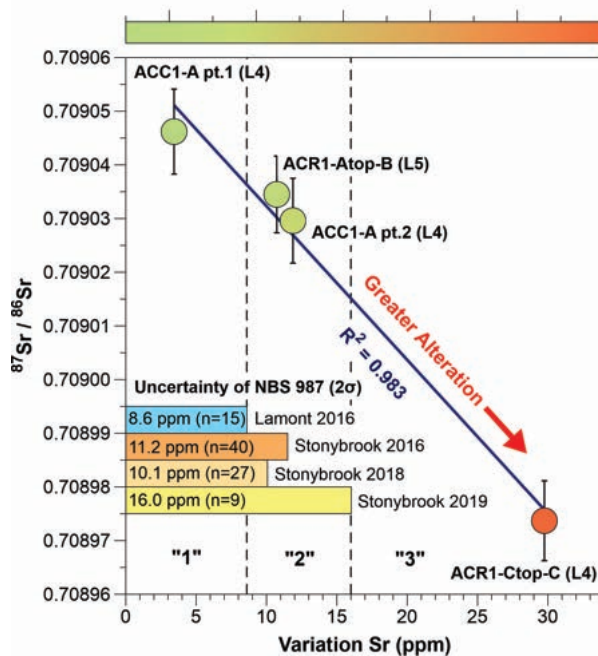
Shells were micro sampled in the best-preserved regions, pri-
 marily through physical micro-drilling using a handheld drill
 and the subsequent powder was homogenized by hand (except
 in the case ACC1-A pt.2, where the shell was carefully frag-
 mented to sand-sized grains and the Sr split was picked under a
 microscope). Minor and trace elements were measured for three
 samples on a Thermo iCap Q quadrupole ICP-MS at LDEO.
 Samples were prepared and analyzed following methods similar
 to Yu et al²⁷. Briefly, ca.250 µg of powder was diluted to 75 ppm

148
149
150
151
152
153
154
155
156
157
158
159
160
161



Supplementary Figure 2: **a)** and **b)** Contact between the unit Cp (lower) and Cs (higher) at the *Caprock* site.

along with the full dissolution splits (Supplementary Table 4 and Supplementary Figure 5). Sr was isolated and dried down using typical separation techniques with Eichon exchange resin. Following separation, 1% of Sr was removed and measured on a mass spectrometer to determine concentration. A drop of 0.05 N Phosphoric acid was added and between 150-375 ng of Sr (for each measurement) was loaded onto degassed Rhenium filaments using tantalum chloride loader.



Supplementary Figure 3: Variation of $^{87}\text{Sr}/^{86}\text{Sr}$ within a leach set (as ppm) vs. the inner leach $^{87}\text{Sr}/^{86}\text{Sr}$ of that shell. Sr leach variation scores are shown by dashed black line; these scores are based on the range of ppm error from seasonal long-term averages of the standard NBS 987. Green circles have low variation within leach sets (usually better preservation) and display younger SIS ages than shell ACR1-Ctop-C (red point) with high variation. This sample is excluded from the average shoreline SIS age based on high Sr variation and other screening criteria (Supplementary Table 3). Long-term uncertainty of standard NBS987 for each year/lab plotted on lower left as ppm variation.

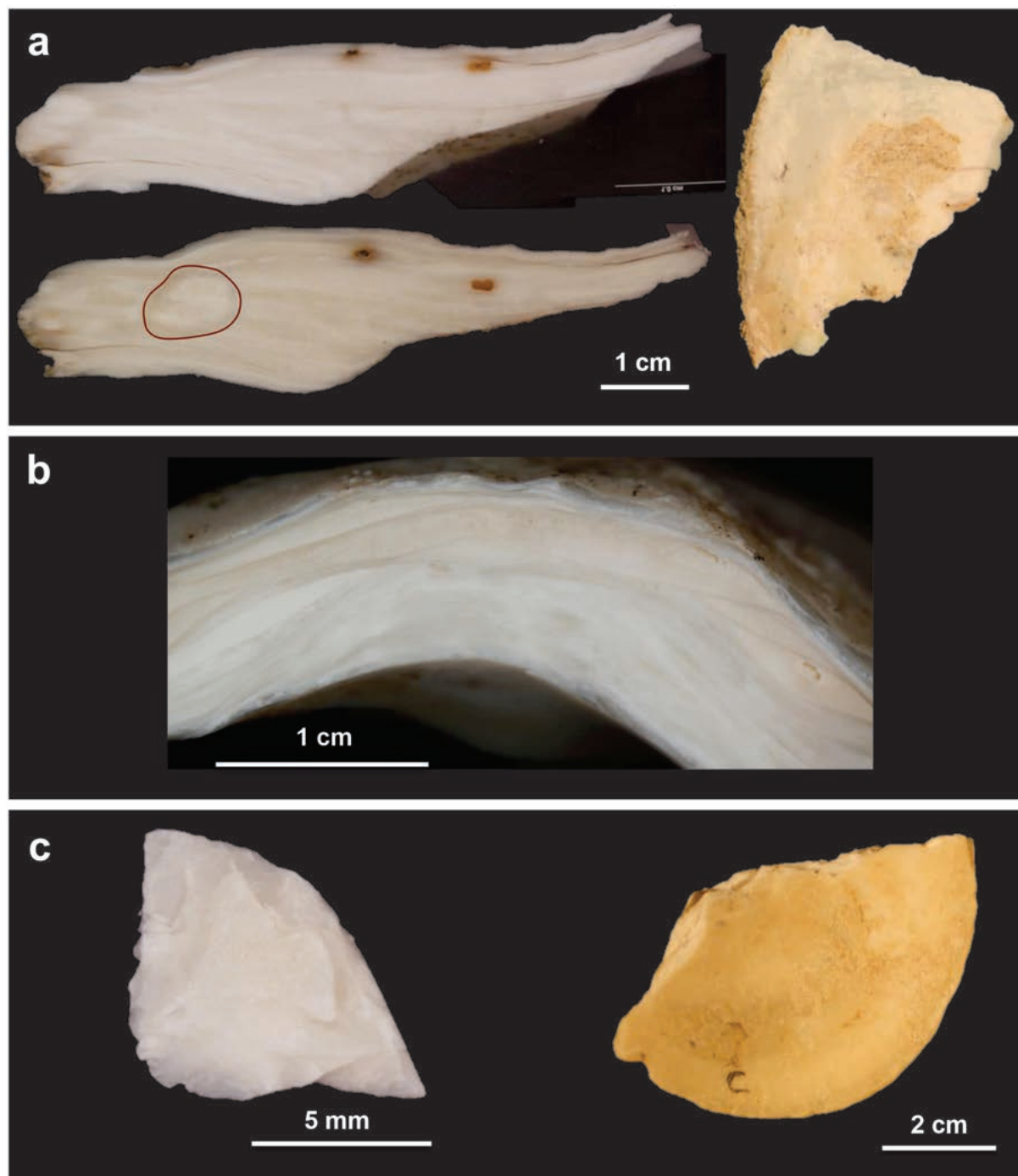
Ca (to negate matrix effects), and run alongside calibration standards covering the range of elements concentrations. The results were normalized to the in-house reference standards QC-Calcite and planktonic standard V03, the latter of which has long-term ($n = 86$) 2σ errors of: Sr/Ca = 1.4%, Mg/Ca = 1.3%, U/Ca = 3.0%, Ba/Ca = 1.8%, Mn/Ca = 1.2%, Al/Ca = 15.8%, Fe/Ca = 2.1% and Na/Ca = 1.3%. A Holocene bivalve (*Tridacna gigas* standard JCT-1) was run alongside the samples for comparison. An elemental scoring system was established for Mg, Mn, and Fe (Supplementary Table 3), elements thought to be indicative of diagenesis^{28;29;26}. Scores ranged from "1" (unaltered) to "3" (altered) based on comparison to a set of Holocene corals and bivalves (for a better overview of screening methods, see Sandstrom et al. (2020)³⁰). Sample splits were taken for Sr isotope analysis (ca. 50 mg for leach fraction, and ca. 10 mg for full dissolution).

Leaching procedures are modified from Bailey et al³¹ (see Hearty et al., 2020²⁶), and involve weak (ca. 0.1M) Acetic acid leaches on the powdered/fragmented shell, designed to preferentially dissolve the more loosely bound secondary $^{87}\text{Sr}/^{86}\text{Sr}$ material before attacking the primary Sr. Typically, four to five leaches were performed per sample, each dissolving ca. 8-12 mg of carbonate (representing 16-25% of the total sample by weight). An additional split (10mg) for each sample was also fully dissolved, as an indication of the average bulk $^{87}\text{Sr}/^{86}\text{Sr}$. Typically, this resulted in 1400-4200 ng of Sr per leach. Only the initial (L1) and inner leaches (defined here as the dissolved 50-80% portions of each sample [i.e. L4 and L5]) were measured,

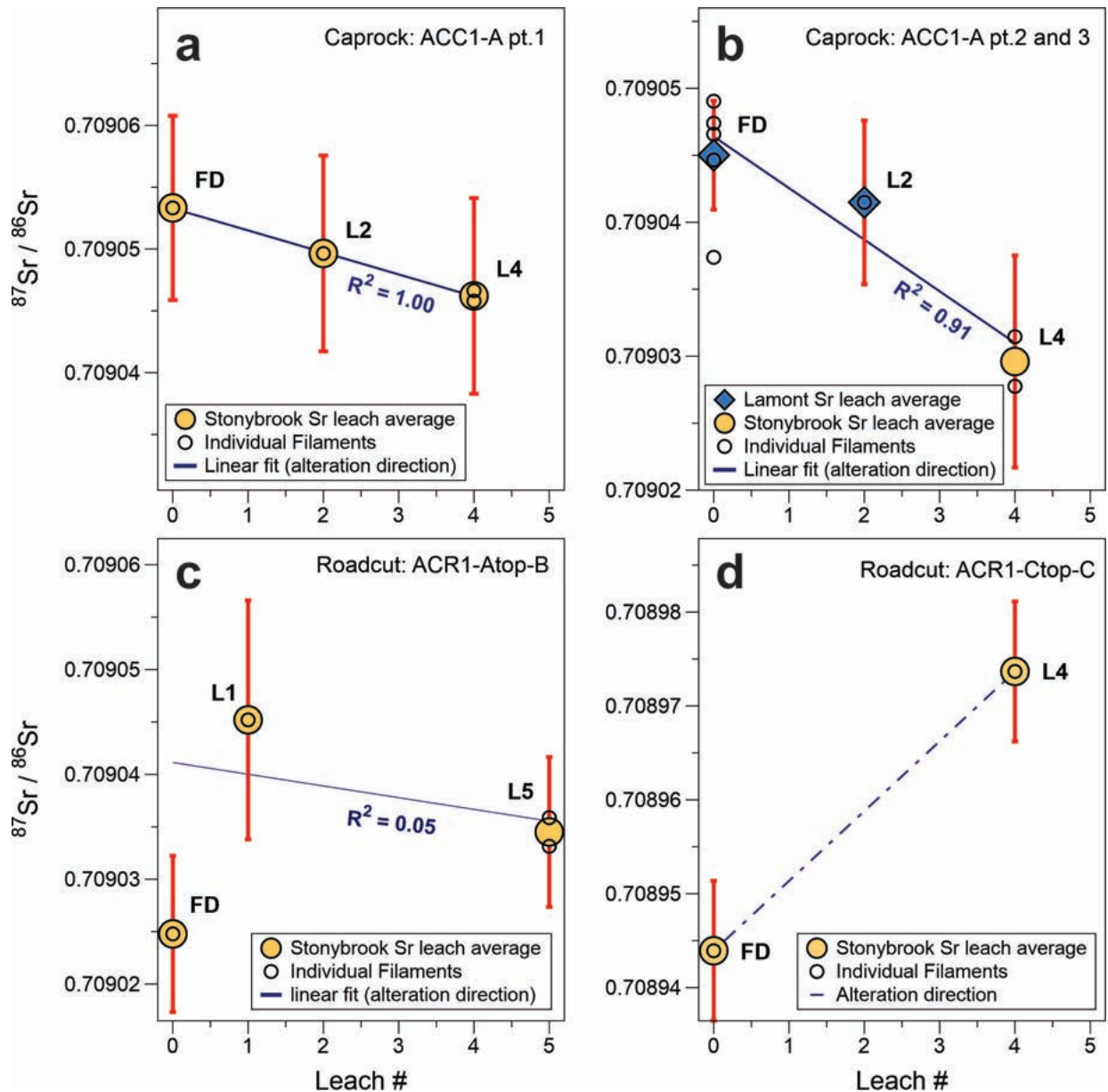
$^{87}\text{Sr}/^{86}\text{Sr}$ ratios were measured on either an IsotopX Phoenix62 Thermal Ionization Mass Spectrometer (TIMS) at Stonybrook University, or a Finnigan Triton Plus TIMS at Lamont-Doherty Earth Observatory (LDEO). Measurements at Stonybrook were conducted in a very similar manner to Gothmann et al²⁹, with a dynamic routine measuring masses 84, 85, 86, 87, and 88 over 160 cycles for each sample. Filaments were slowly ramped up to 2.8 - 3.2 A and a temperature of ca. 1400 degrees Celsius, to achieve a beam intensity between 3-5 V on mass 88. TIMS measurements at LDEO were carried out using a static routine for 200-400 cycles with similar parameters to Stonybrook. The Sr isotope external standard NBS SRM 987 long-term instrument accuracy at the two labs was computed every season and ranged between 8.6 - 16 ppm (2σ) (Supplementary Figure 3). At Stonybrook: NBS 987 = 0.710245 ± 0.000008 (2σ ; 2016, $n = 40$); 0.709241 ± 0.000007 (2σ ; 2018, $n = 27$), and

214 0.710244 ± 0.000011 (2σ ; 2019, n =9) and at LDEO: NBS 987
215 $= 0.710238 \pm 0.000006$ (2σ ; 2016, n = 15). Sr isotopes were all
216 corrected for mass fractionation based on an $^{86}\text{Sr}/^{88}\text{Sr}$ ratio of
217 0.1194 and normalized to the accepted NBS 987 standard value
218 $= 0.709248$. Sr isotope stratigraphy ages were calculated using
219 the LOWESS version 5 curve from McArthur et al²⁸.

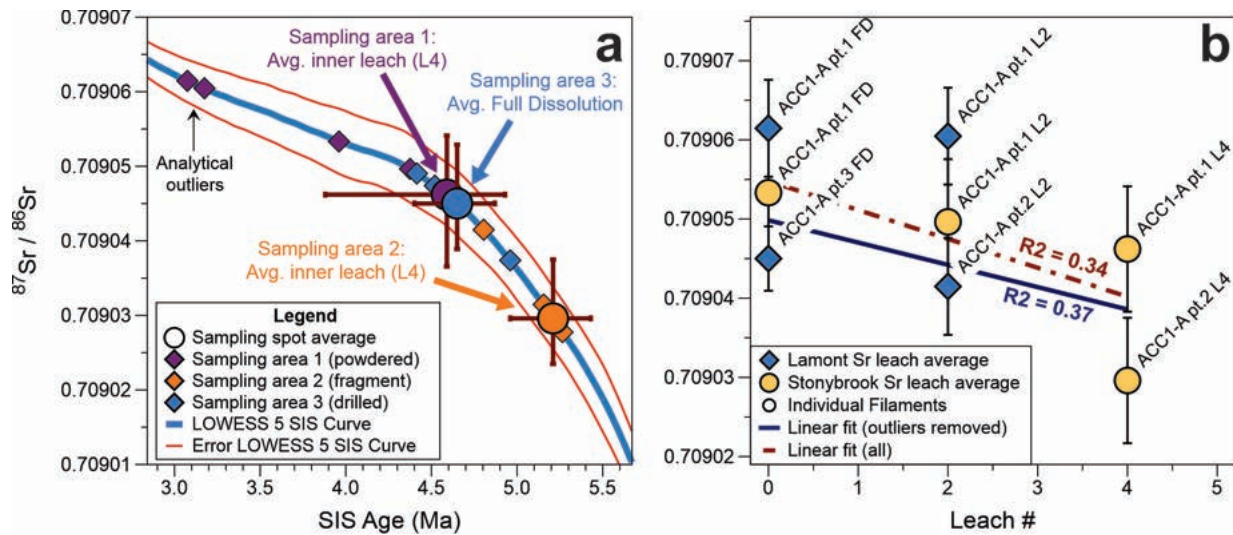
220 Sr isotope variations were calculated as ppm within leach sets (as
221 the total range of $^{87}\text{Sr}/^{86}\text{Sr}$ values within a leach set, multiplied
222 by a million to read as ppm) for each sample (Supplementary
223 Table 3). A scoring system from "1" to "3" was established based
224 on long-term uncertainties of NBS 987, where samples with Sr
225 isotope variations $< 8.6\text{ppm} = 1$, between 8.6-16 ppm = 2, and $>$
226 16 ppm = 3 (see Supplementary Figure 3, Supplementary Table
227 3 and Sandstrom et al., 2020³⁰).



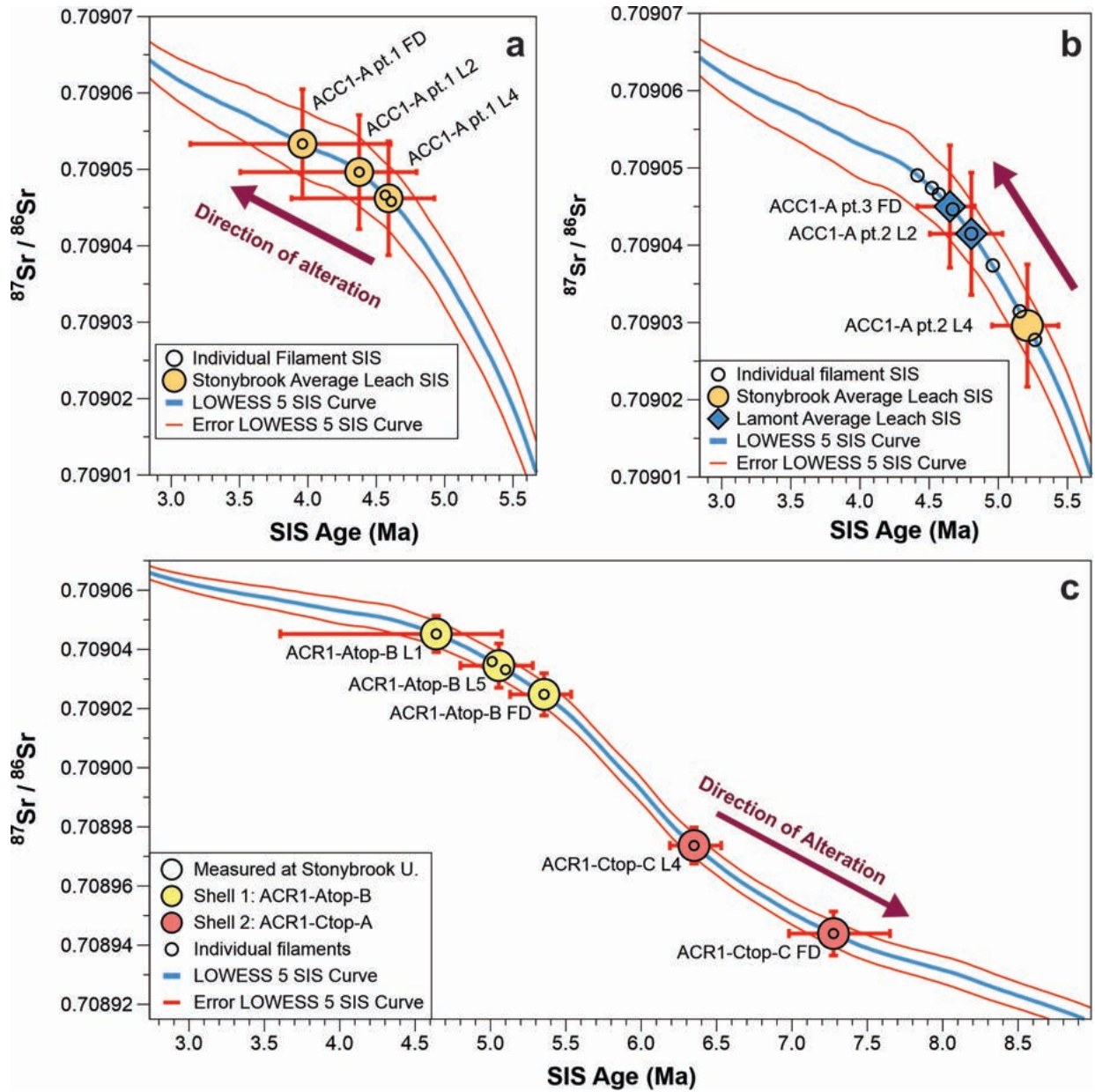
Supplementary Figure 4: Sample images. **a)** Oyster shell ACC1-A, showing slabbed x-section (top left), part 3 drill location (bottom left), and original shell fragment (right). **b)** Sample ACR1-Atop-B slabbed x-section. **c)** Shell ACR1-Ctop-C showing fragment used in Sr isotope dating (left) and partial shell collected from the field (right).



Supplementary Figure 5: Sr isotope leach set data for individual sample areas. Red error bars represent 2σ external uncertainty of NBS987 (except for full dissolution ACC1-A pt.3 FD, which is 2σ standard error of the mean). Linear regression lines (blue) indicate direction of alteration, with altering fluids causing the *Caprock* oyster (**a** and **b**) to appear slightly younger (more radiogenic $^{87}\text{Sr}/^{86}\text{Sr}$), and the *Roadcut* samples (**c** and **d**) to appear older (alteration fluid with low $^{87}\text{Sr}/^{86}\text{Sr}$). **a** and **b**) Leach set data for sample ACC1-A parts 1 and 2 showing less radioactive $^{87}\text{Sr}/^{86}\text{Sr}$ (increased SIS age) with better preservation (L4). **c**) The inner leach lies between the initial leach and full dissolution, overlapping both within uncertainty. The leach set suggests alteration fluids cause ages to appear younger, while the full dissolution indicates the opposite. However, based upon the excellent preservation index score, the inner leach (L5) most likely reflects the original Sr isotopic ratio. **d**) The trend of significantly increasing $^{87}\text{Sr}/^{86}\text{Sr}$ of the inner leach compared to the full dissolution indicates post-depositional alteration in this sample.



Supplementary Figure 6: **a)** Oyster shell ACC1-A (*Caprock*) detailed Sr isotopes and SIS age assignments from three different sampling locations. **b)** Leach Sr values and different TIMS machines (yellow = stonybrook, blue = Lamont). Sample splits ACC-1A pt.1 FD and L2 measured at LDEO appear to be outliers for reasons unknown [possibly turret related? as this was the first turret run?]. Repeated measurements on these same splits at SBU yielded more reliable $^{87}\text{Sr}/^{86}\text{Sr}$ values that more closely align with other measurements from different sections of this shell, both at SBU and LDEO. Linear regression was computed for all leach averages (red) and also excluding the two outliers (blue) with similar results. There is a slight trend toward less radiogenic values for the better preserved inner leach measurements.



Supplementary Figure 7: Same data as Supplementary Figure 5. Sr isotope leach set data for individual sample areas, plotted against Lowess5 SIS curve. Red error bars represent 2σ external uncertainty of NBS987 (except for full dissolution ACC1-A pt.3 FD, which is 2σ standard error of the mean). Purple arrows indicate direction of alteration, with altering fluids causing the *Caprock* oyster (panels a and b) to appear younger (more radioactive $^{87}\text{Sr}/^{86}\text{Sr}$), and the *Roadcut* samples (panel c) to appear older (in the case of ACR1-Ctop-C), and possibly younger in the case of ACR1-Atop-A, but no distinct trend can be assigned.

Supplementary Table 3: Elemental and diagenetic screening results of oyster samples. BDL = below detection limit. n.a. = not measured. ^a Jct-1 is the Holocene Tridactna standard³². ^b Samples used in elemental score average. ^c Full dissolution used for variation calculation, as L1 was not measured. ^d Scoring criteria outlined in Sandstrom et al. (2020)³⁰. ^e See Supp. methods and Hearty et al. (2020)²⁶. ^f Leach variation scores: "1" = <8.6ppm; "2" = 8.6 to 16 ppm; "3" = >16 ppm. ^g Samples with preservation index scores \geq "2" are considered altered and excluded.

Sample code	ACC1-A pt.1	ACR1-Atop-B	ACR1-Ctop-C	Jct-1 ^a
SESAR IGSN ID	IEMRS006J	IEMRS006L	IEMRS006P	N/A
Description	Caprock - Oyster	Roadcut - Oyster	Roadcut - Oyster	Holocene Tridactna
Na/Ca (mmol/mol)	8.1	9.5	11.7	19.9
Mg/Ca (mmol/mol) ^b	2.9	3.3	4.9	1.2
Al/Ca (μ mol/mol)	4.6	BDL	20.4	17.2
Mn/Ca (μ mol/mol) ^b	78.8	16.2	1484.7	2.6
Fe/Ca (μ mol/mol) ^b	1.7	BDL	144.5	BDL
Sr/Ca (mmol/mol)	0.58	0.85	1.50	1.84
Ba/Ca (μ mol/mol)	2.2	2.2	5.9	1.6
U/Ca (nmol/mol)	89.2	107.5	155.2	33.3
number of splits	1	2	1	3
⁸⁷ Sr/ ⁸⁶ Sr leach variation (ppm)	11.88	10.73	29.75 ^c	n.a.
Elemental score (1-3) ^d	1.67	1.67	2.33	1.00
SEM score (1-3) ^e	2	n.d.	2	n.a.
Optical score (1-3) ^e	2	1	2	1
⁸⁷ Sr/ ⁸⁷ Sr variation score (1-3) ^f	2	2	3	n.a.
Preservation Index Score^g (average of all scores: 1-3)	1.92	1.56	2.33	1.00

Supplementary Table 4: $^{87}\text{Sr}/^{86}\text{Sr}$ results and Sr isotope stratigraphy ages for Caprock and Roadcut outcrops. ^a Inner leach Sr isotope values for sample; ^b Sample leaches excluded based on analytical or diagenetic criteria; ^c Sample excluded from shoreline age based on significant diagenesis (see Table S3); ^d Uncertainty based on 2σ SEM; ^e Sample variation is calculated as the difference between the initial leach [or full dissolution] and last leach, multiplied by one million (ppm); ^f Average of inner leaches on samples that passed screening criteria: ACC1-A pts. 1 and 2, and ACR1-Atop-B; ^g Uncertainty based on combined analytical [2σ SEM] and SIS curve [LOWESS 5] errors.

Sample Name	TIMS Lab	Leach ID	Nb. filaments	$^{87}\text{Sr}/^{86}\text{Sr}$ (measured)	$^{87}\text{Sr}/^{86}\text{Sr}$ (normalized to NBS97)	2σ external uncertainty	Mean SIS Age (Ma)	Maximum SIS Age (Ma)	Minimum SIS Age (Ma)	Uncorrected SIS Age (Ma)
Average $^{87}\text{Sr}/^{86}\text{Sr}$ by Leach										
Caprock										
ACC1-A pt.1 FD	SBU	FD	1	0.7090465	0.7090533	0.0000075	3.960	4.605	3.140	4.58
ACC1-A pt.1 L2	SBU	L2	1	0.7090462	0.7090496	0.0000079	4.375	4.795	3.505	4.59
ACC1-A pt.1 L4 ^a	SBU	L4	2	0.7090427	0.7090462	0.0000079	4.590	4.925	3.880	4.76
ACC1-A pt.1 FD ^b	LDEO	FD	1	0.7090509	0.7090615	0.0000061	3.075	3.745	2.635	4.27
ACC1-A pt.1 L2 ^b	LDEO	L2	1	0.7090499	0.7090605	0.0000061	3.175	3.855	2.695	4.36
ACC1-A pt.2 L2	LDEO	L2	1	0.7090309	0.7090415	0.0000061	4.805	5.030	4.505	5.17
ACC1-A pt.2 L4 ^a	SBU	L4	2	0.7090261	0.7090296	0.0000079	5.210	5.435	4.955	5.32
ACC1-A pt.3 FD	LDEO	FD	5	0.7090345	0.7090344	0.0000041 ^d	4.650	4.415	4.830	5.055
Roadcut										
ACR1-Atop-B FD	SBU	FD	1	0.7090180	0.7090248	0.0000075	5.355	5.535	5.130	5.52
ACR1-Atop-B L1	SBU	L1	1	0.7090409	0.7090452	0.0000114	4.640	5.075	3.605	4.83
ACR1-Atop-B L5 ^a	SBU	L5	2	0.7090279	0.7090345	0.0000072	5.055	5.280	4.800	5.27
ACR1-Ctop-C FD	SBU	FD	1	0.7089371	0.7089439	0.0000075	7.275	7.650	6.980	7.62
ACR1-Ctop-C L4 ^{a,c}	SBU	L4	1	0.7089668	0.7089737	0.0000075	6.350	6.530	6.190	6.52
Average Shoreline SIS Age										
Average of screened inner leaches ^f	SBU	L4, L5	6	0.7090322	0.7090368	0.0000064 ^d	4.98	5.225 ^e	4.685 ^e	5.13

228 REFERENCES

- 229 [1] Darwin, C. *Geological observations on South America: Being the third part of the geology of the voyage of the*
 230 *Beagle, under the command of Capt. Fitzroy, RN during*
 231 *the years 1832 to 1836* (Smith, Elder and Company, 65,
 232 Cornhill., 1846).
 233
- 234 [2] Feruglio, E. *I terrazzi marini della Patagonia* (Cooperativa
 235 Tip. Edit. Paolo Galeati, 1933).
- 236 [3] Feruglio, E. *Descripción geológica de la Patagonia*, vol. 1
 237 (Impr. y Casa Editora "Coni", 1949).
- 238 [4] Schellmann, G. & Radtke, U. Coastal terraces and
 239 holocene sea-level changes along the patagonian atlantic
 240 coast. *Journal of Coastal Research* 983–996 (2003).
- 241 [5] Zanchetta, G. *et al.* Middle-to late-holocene relative sea-
 242 level changes at puerto deseado (patagonia, argentina). *The*
 243 *Holocene* **24**, 307–317 (2014).
- 244 [6] Bini, M. *et al.* Markers of palaeo sea-level in rocky coasts
 245 of patagonia (argentina). *Rendiconti Online della Società*
 246 *Geologica Italiana* **20**, 10–14 (2013).
- 247 [7] Fucks, E. *et al.* Influence of quaternary sea level changes in
 248 the littoral of chubut, argentina. *Journal of South American*
 249 *Earth Sciences* **88**, 589–598 (2018).
- 250 [8] Pappalardo, M. *et al.* Challenges in relative sea-level
 251 change assessment highlighted through a case study: The
 252 central coast of atlantic patagonia. *Global and Planetary*
 253 *Change* **182**, 103008 (2019).
- 254 [9] Pappalardo, M. *et al.* Coastal landscape evolution and
 255 sea-level change: A case study from central patagonia
 256 (argentina). *Zeitschrift für Geomorphologie* **59**, 145–172
 257 (2015).
- 258 [10] Rostami, K., Peltier, W. & Mangini, A. Quaternary marine
 259 terraces, sea-level changes and uplift history of patago-
 260 nia, argentina: comparisons with predictions of the ice-4g
 261 (vm2) model of the global process of glacial isostatic ad-
 262 justment. *Quaternary Science Reviews* **19**, 1495–1525
 263 (2000).
- 264 [11] Pedoja, K. *et al.* Uplift of quaternary shorelines in eastern
 265 patagonia: Darwin revisited. *Geomorphology* **127**, 121–
 266 142 (2011).
- 267 [12] Schellmann, G. & Radtke, U. ESR dating stratigraphically
 268 well-constrained marine terraces along the patagonian at-
 269 lantic coast (argentina). *Quaternary International* **68**, 261–
 270 273 (2000).
- 271 [13] Rutter, N. *et al.* Correlation and dating of quaternary
 272 littoral zones along the patagonian coast, argentina. *Qua-*
 273 *ternary Science Reviews* **8**, 213–234 (1989).
- 274 [14] Del Río, C., Griffin, M., McArthur, J., Martínez, S. &
 275 Thirlwall, M. Evidence for early pliocene and late miocene
 276 transgressions in southern patagonia (argentina): 87sr/86sr
 277 ages of the pectinid "chlamys" actinodes (sowerby). *Jour-*
 278 *nal of South American Earth Sciences* **47** (2013).
- 279 [15] del Río, C. J., Martínez, S. A. & Scasso, R. A. Nature
 280 and origin of spectacular marine miocene shell beds of
 281 northeastern patagonia (argentina): Paleoecological and
 282 bathymetric significance. *Palaios* **16**, 3–25 (2001).
- [16] Dozo, M. T. *et al.* Late miocene continental biota in north-
 283 eastern patagonia (península valdés, chubut, argentina).
 284 *Palaeogeography, Palaeoclimatology, Palaeoecology* **297**,
 285 100–109 (2010).
 286
- [17] Farinati, E. & Zavala, C. Trace fossils on shelly substrate.
 287 an example from the miocene of patagonia, argentina. *Acta*
 288 *Geologica Hispanica* **37**, 29–36 (2002).
 289
- [18] del Río, C. J. Tertiary marine molluscan assemblages of
 290 eastern patagonia (argentina): a biostratigraphic analysis.
 291 *Journal of Paleontology* **78**, 1097–1122 (2004).
 292
- [19] Bigazzi, G., Bonadonna, F., Leone, G. & Zanchetta, G.
 293 Primeros datos geoquímicos y geocronológicos a partir
 294 de algunas cineritas del area bonarense (1995).
 295
- [20] Farinati, E. A. & Zavala, C. A. Asociaciones de
 296 megafósiles de invertebrados en el neógeno atlántico de la
 297 patagonia argentina (2005).
 298
- [21] Lema, H. A. *et al.* Hoja geológica 4566-ii y iv camarones
 299 (2001).
 300
- [22] Bini, M. *et al.* Mid-holocene relative sea-level changes
 301 along atlantic patagonia: new data from camarones, chubut,
 302 argentina. *The Holocene* **28**, 56–64 (2018).
 303
- [23] Schellmann, G. *Jungkänozoische Landschaftsgeschichte*
 304 *Patagoniens (Argentinien): andine Vorlandvergletscherun-*
 305 *gen, Talentwicklung und marine Terrassen* (1. Auflage,
 306 Essen: Klartext, 1998, 1998).
 307
- [24] McArthur, J. M. Recent trends in strontium isotope stratig-
 308 raphy. *Terra nova* **6**, 331–358 (1994).
 309
- [25] Cochran, J. K. *et al.* Effect of diagenesis on the sr, o, and
 310 c isotope composition of late cretaceous mollusks from
 311 the western interior seaway of north america. *American*
 312 *Journal of Science* **310**, 69–88 (2010).
 313
- [26] Hearty, P. J. *et al.* Pliocene-pleistocene stratigraphy and
 314 sea-level estimates, republic of south africa with implica-
 315 tions for a 400 ppmv co2 world. *Paleoceanography and*
 316 *Paleoclimatology* **n/a**, n/a (2020).
 317
- [27] Yu, J., Day, J., Greaves, M. & Elderfield, H. Determina-
 318 tion of multiple element/calcium ratios in foraminiferal
 319 calcite by quadrupole icp-ms. *Geochemistry, Geophysics,*
 320 *Geosystems* **6** (2005).
 321
- [28] McArthur, J., Howarth, R. & Shields, G. Strontium isotope
 322 stratigraphy. *The geologic time scale* **1**, 127–144 (2012).
 323
- [29] Gothmann, A. M. *et al.* Fossil corals as an archive of
 324 secular variations in seawater chemistry since the mesozoic.
 325 *Geochimica et Cosmochimica Acta* **160**, 188–208 (2015).
 326
- [30] Sandstrom, M. R. *et al.* Age constraints on surface
 327 deformation recorded by fossil shorelines at Cape
 328 Range, Western Australia. *GSA Bulletin* (2020). URL
 329 <https://doi.org/10.1130/B35564.1>. <https://pubs.geoscienceworld.org/gsabulletin/article-pdf/doi/10.1130/B35564.1/5135376/b35564.pdf>.
 330
 331
 332
 333
- [31] Bailey, T., McArthur, J., Prince, H. & Thirlwall, M. Disso-
 334 lution methods for strontium isotope stratigraphy: whole
 335 rock analysis. *Chemical Geology* **167**, 313–319 (2000).
 336

- 337 [32] Watanabe, T., Suzuki, A., Kawahata, H., Kan, H. & Ogawa,
338 S. A 60-year isotopic record from a mid-holocene fossil
339 giant clam (*tridacna gigas*) in the ryukyu islands: physio-
340 logical and paleoclimatic implications. *Palaeogeography,*
341 *Palaeoclimatology, Palaeoecology* **212**, 343–354 (2004).